Universiteit Utrecht

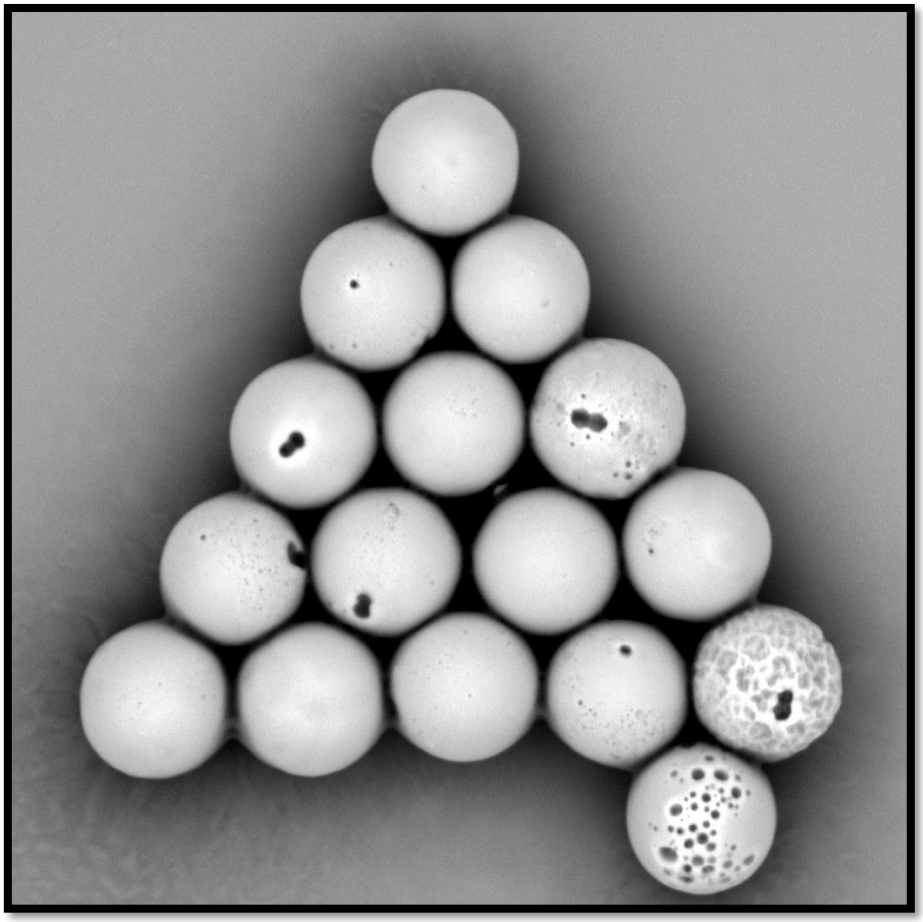

The Quest for the Luminescent Photonic Crystal

Formation of Monodisperse Supraparticles from Microfluidics Directed Self-assembly of Quantum Dots

Luke Chadwick, Federico Montanarella, Daniel VanMaekelbergh, Alfons Van Blaaderen

CONDENSED MATTER AND INTERFACES GROUP | UTRECHT UNIVERSITY

Contents

Introduction

A nanomaterial is generally defined as a material with structural components sized between 1 – 1000nm in at least one dimension.[1] Nanoscience is the study of nanomaterials and it is a broad field with a comprehensive list of specialised terminology for referring to the different categories and sub categories of nanomaterials. Different types of nanomaterials are usually distinguished either by size, morphology or physical and chemical properties. Nanomaterials can be crystalline or amorphous and crystalline materials are referred to as nanocrystals (NCs). A nanomaterial can be classified as 0, 1, 2 or 3 dimensional depending on how many of its external dimensions are confined to the nanoscale (measures <1000nm). An example of a 0-dimensional material is a nanoparticle (NP), which refers to an object that is confined to the nanoscale in all three dimensions, whose longest and shortest axes don't differ significantly. Common 1-dimensional materials include nanowires, nanorods and nanotubes, all of which exceed the nanoscale in 1 dimension. 2-dimensional materials include nanosheets or nanofilms, which are thin layers of material with a thickness less than 1000nm but that extend over 1000nm in the other two dimensions. 3-dimensional materials, also called bulk nanomaterials, can refer to a material that, as a whole is not confined to the nanoscale in any dimension, but it possesses components or features that are confined, for example a large crystal composed of nanoparticles or a stack of nanofilms with a thickness greater than 1000nm. There is great interest in the field of nanoscience because nanomaterials have different properties compared to a bulk material and their physical and chemical properties are size dependent. For example, if a catalytic material is divided into NPs, the speed of the catalytic process will increase, as many more reaction sites are available due to the much greater surface area.[2] Another example is the size dependent band gap of semiconductor nanomaterials. The origin of these special properties is from two fundamental nanoscale effects. (1) The increase in the ratio of surface to bulk atoms as the size of the material decreases and (2) spatial confinement effects.

The reason an increase in the ratio of surface to bulk atoms changes the properties of a material is due to the fact that surface atoms behave differently to bulk atoms because they have fewer neighbours, leading to unsatisfied chemical bonds known as dangling bonds. As a result, surface atoms have a higher free energy, higher reactivity and higher mobility.[3] So as size decreases, the number of surface atoms relative to bulk atoms increases and the contribution of the surface atoms to the total free energy and the properties of the material increases. This causes melting and evaporation temperatures to decrease, while reactivity, elasticity and plasticity are increased.

Spatial confinement effects arise from the quantum mechanical nature of matter, which goes unnoticed in macroscopic objects but becomes increasingly important as the size of material decreases below a certain critical limit. This limit differs depending on the material and the property. An important example for this project is the effect of spatial confinement in semiconductor materials, known as quantum confinement. In a semiconductor material, if an electron in the valence band absorbs enough energy it is promoted to a higher energy state in the conduction band. The vacancy created in the valence band is known as a hole and an electron-hole pair is referred to as an exciton. The spatial extension of excitons, known as the Bohr radius (a_0), is characteristic of a material and ranges from 2-50nm.[4] When a materials dimensions approach a_0, confinement begins to affect the exciton wave function, inducing changes in the electronic states that result in an increase of the band gap energy with decreasing size.[5] This is the reason for the size and shape dependent optoelectrical properties of semiconductor nanocrystals. This allows fine tuning of the photoluminescence (PL) properties that arise from exciton formation and recombination, by absorption and emission of photons.

A property of NPs that is particularly important for this project is that their size allows them to form a colloidal suspension when dispersed in an appropriate liquid solvent. This is because NPs are small enough to experience random Brownian motion due to continuous bombardment from solvent molecules. This property is fundamental to the self-assembly process that is explored in this project. The combination of individual nanomaterial components into assemblies can create structures with unique properties. For example, theoretical calculations have predicted that arranging semiconductor nanocrystals into 2D honeycomb superlattices results in both valence and conduction bands that can be filled with Dirac-type charge carriers with strong spin-orbit coupling, which allows the material to behave either like a zero-bandgap material or topological-insulator electronically.[6,7] The potential to create new materials in this way has created much interest in NP assembly processes and how they can be controlled and optimised to create a myriad of novel structures with interesting and desirable properties. This has become a very important sub-topic within nanomaterial research. Methods for creating nanostructures are divided into two general groups, top-down methods and bottom-up methods. Top-down methods involve the breaking up of bulk material into nanosized structures. Bottom-up approaches involve using chemical synthesis and self-assembly to create nanosized structures. Top-down methods can be useful, particularly for large scale processes, but there are limits to the complexity of structures that can be formed and methods such as lithography are reaching their limits in terms of resolution.[8] For this reason bottom-up self-assembly processes are being explored as the route to new, more complex structures that are not achievable with top-down methods.

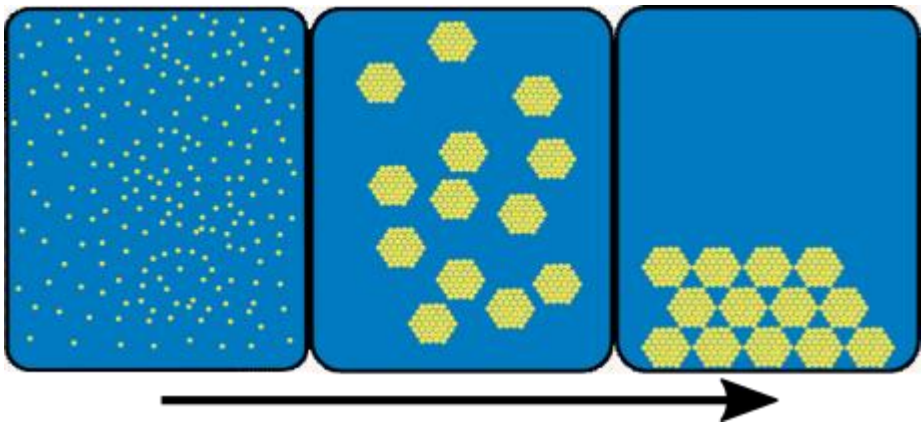

Figure 1. Schematic example of hierarchical self-assembly process, showing the progression from NCs, to SPs, to photonic crystal.

The aim of this project is to create a structure that combines the photoluminescent properties of semiconductor NCs with the photonic properties of a photonic crystal. The building blocks of a photonic crystal must be sized on the same scale as wavelengths of light so semiconductor NCs are too small for this purpose. Instead we plan to realise the photonic crystal through the self-assembly of crystalline colloidal assemblies of NCs, known as supraparticles (SPs). That is to say, we wish to make crystals of crystals of nanocrystals (Fig.1). This is an interesting structure to try and make because the photoluminescent properties of the NCs could enhance the photonic properties of the photonic crystal and arranging the NCs in such an ordered structure may improve the out-coupling of the emitted light. Ideally, the photonic crystal created would have a photonic band gap (PBG) that overlaps as much as possible with the emission spectrum of the quantum dots. To create such a material, a reliable and controllable process for the creation of monodisperse SPs is necessary, as it would allow for the tuning of the PBG. This project focuses on developing such a process. Unfortunately, in the end we did not achieve the goal of making a photonic crystal during this project, but from this work we have gained a better understanding of the parameters that have the largest

impact on the quality of the SPs produced using the specific method chosen, thus coming a step closer to the realization of these structures.

Theory

This project has three distinct steps. The first is the synthesis and characterization of monodisperse semiconductor NCs, also known as quantum dots (QDs). The second is creating monodisperse SPs from the QDs. The final step is to create a photonic crystal through the self-assembly of colloidal SPs. The following section will clearly define QDs, SPs and photonic crystals. We will also provide background information on the synthesis methods used during the project and the theory behind the self-assembly of colloidal particles.

Photonic Crystals

A photonic crystal (PC) is defined as an ordered structure with periodicity on the same scale as wavelengths of light. PCs are observed in nature as opals and their ability to manipulate light is exploited by certain animals who have developed evolutionary adaptions.[9] A familiar example are the feathers of a peacock which owe their bright iridescent colouring to nanoscale melanin rods on their surface, which act as a PC and strongly reflect light of certain wavelengths (Fig.2).[10] This is an example of one of the novel optical properties of PCs called structural coloration, when structural features of an object create colour due to interference of visible light reflected by the object. Photonic crystals can also be used as waveguides and omni-directional reflectors. Their optical properties make them attractive for applications in areas such as the optimization of photovoltaic devices[11], fibre-optics[12] and as optical transistors for optical computing.[13]

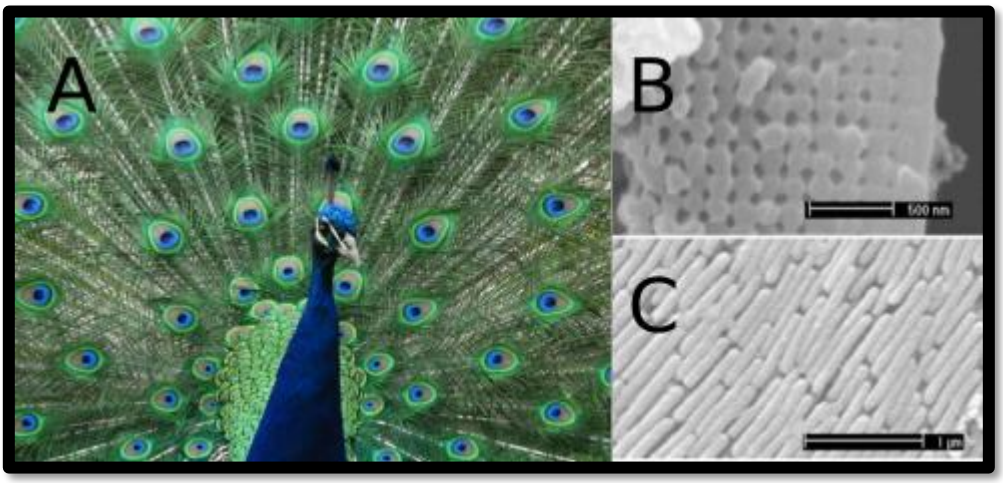

Figure 2. (A)Photograph of peacock.(B,C) SEM images of nanoscale melanin rods on the surface of the peacock's feathers that are responsible for the bright iridescent colouring.[10]

The origin of the optical properties of a PC can be compared to the origin of the electronic properties of a regular crystal. When the word crystal is used, it typically refers to a periodic arrangement of atoms or molecules. The pattern created by this periodic arrangement is known as the crystal lattice. The atoms/molecules of the lattice present a periodic potential. Electrons travelling through the lattice are scattered by this potential. Electrons propagate as waves, which are periodic in nature, and the wavelength corresponds to the energy of the electron. Electrons with wavelengths matching the periodicity of the lattice are strongly scattered and are unable to propagate through the

crystal. This is the origin of the band gap in semiconductor materials.[14] Photonic crystals can be described as the optical analogue to this system. Larger objects of a size comparable to wavelengths of light replace the atoms and molecules and photons replace the electrons as they also propagate as waves. This creates a structure in which the refractive index changes periodically due to the differing dielectric constants of the repeating regions of the crystal. Light is refracted and reflected at each interface between these regions. Light waves refracted or reflected from different interfaces interfere with each other. The wavelength of the light and the distance between interfaces determines whether interference is constructive or destructive. The net result of this interference is that propagation through the crystal is forbidden for certain wavelengths, creating a PBG.[15] Interference between reflected wavelengths in the visible part of the region gives rise structural colouration.[9]

Supraparticles

The second step in this project is the fabrication of SPs, which can be defined as colloidal clusters of NPs that consist of a well-controlled number of particles. There are two main routes by which SPs can be formed, a solvothermal method[16–18] or an emulsion-based method.[19] The solvothermal route is generally a single step method by which nanoparticles are formed in solution and then self-assembly into colloidal clusters is induced by changes in the chemical conditions of the system. The emulsion-based method generally has two steps as first the NPs must be synthesized and then the nanocrystal solution is used to create an emulsion in which the NP solution is the Dispersed phase and then self-assembly of NPs inside the droplets is induced by evaporation of the solvent.

SPs have piqued the interest of many researchers because they exhibit properties that differentiate them from individual NPs and larger 2/3D superstructures. For example, the larger size of SPs compared to their constituent NPs make them easier to process in an industrial setting and SPs are highly dispersible in solution compared to superstructures formed on a solid substrate or interface. SPs can be constructed from a large number of identical particles or a collection of different types of particles but in both cases, SPs have collective and or synergistic properties not present in the individual NPs. For example Ge et al[16] produced SPs with unique magnetic properties through the self-assembly of Fe_3O_4 NCs with diameters of about 8nm. For Fe_3O_4 material, the critical size for the superparamagnetic-ferromagnetic transition is around 30nm so the primary Fe_3O_4 NCs are superparamagnetic. At room temperature, the SPs produced are also superparamagnetic, but they have a much greater magnetic moment compared to the individual NCs due to their larger size. The magnetic moment for a SP with a diameter of 174nm is almost 10^4 times larger than that of an individual NC. These particles are highly responsive to an external magnetic field, which is an important property for biomedical applications.

QDs are known for their excellent photoluminescent properties, with versatile size tuneable emission and a quantum yield close to unity. Montanarella et al[20] demonstrate how different types of QDs can be combined into SPs with highly versatile optical properties. This was achieved by creating SPs from a combination of red, green and blue emitting QDs. By carefully controlling the relative amounts of each type of QD in the SP, emission could be tuned from pure colours to a broad white light spectrum. The versatile optical properties of these SPs mean they have potential for applications as phosphors in LEDs, opto-electronic integration in semiconductor chips and as biological labels. Li et al[21] used a solvothermal procedure to create highly monodisperse SPs form CdS NCs. The procedure could be altered to control the size of the SPs produced and sizes could be tuned from 80 to 500nm. The size and monodispersity of the SPs allowed them to be self-assembled into thin film photonic crystals that exhibit structural colouration dependent on the size of the SPs. The magneto- fluorescent SPs created by Bawendi et al[22] combine the optical properties of QDs with the magnetic properties of metallic NCs to create SPs great potential in advanced biomedical applications. A simple synthesis

method sees the assembly of Fe_3O_4 NCs with CdSe/CdS core/shell QDs to form SPs with a densely packed magnetic core surrounded by a fluorescent shell. These examples clearly demonstrate why SPs are interesting structures to create.

Quantum Dots

CdSe/CdS Core/Shell Heteronanocrystals

The first step of this project concerns the synthesis of monodisperse QDs that will serve as the fundamental building blocks for the hierarchical self-assembly process. We chose to work with CdSe/CdS core/shell QDs because it is a well-known system with high reproducibility, good stability and they have desirable optical properties including high quantum yield and tuneable emission.[23–28] QDs are 0-dimensioinal semiconductor NPs. If a photon with energy greater than the band gap of semiconductor material comes in contact with the material, it will be absorbed, promoting an electron from the valence band to the conduction band. For the electron to fall back to its lower energy state in the valence band it must emit a photon. This process of absorbing and emitting photons is referred to as photoluminescence (PL). CdSe is a semiconductor material with a bulk band gap of 1.74 eV, which corresponds to PL emission in the NIR part of the electromagnetic spectrum. For crystals smaller than 10nm in diameter, the energy of the band gap increases due to quantum confinement (Fig. 3) so CdSe can be used to produce particles that absorb and emit light across nearly the entire spectrum of visible light, depending on their size.[4]

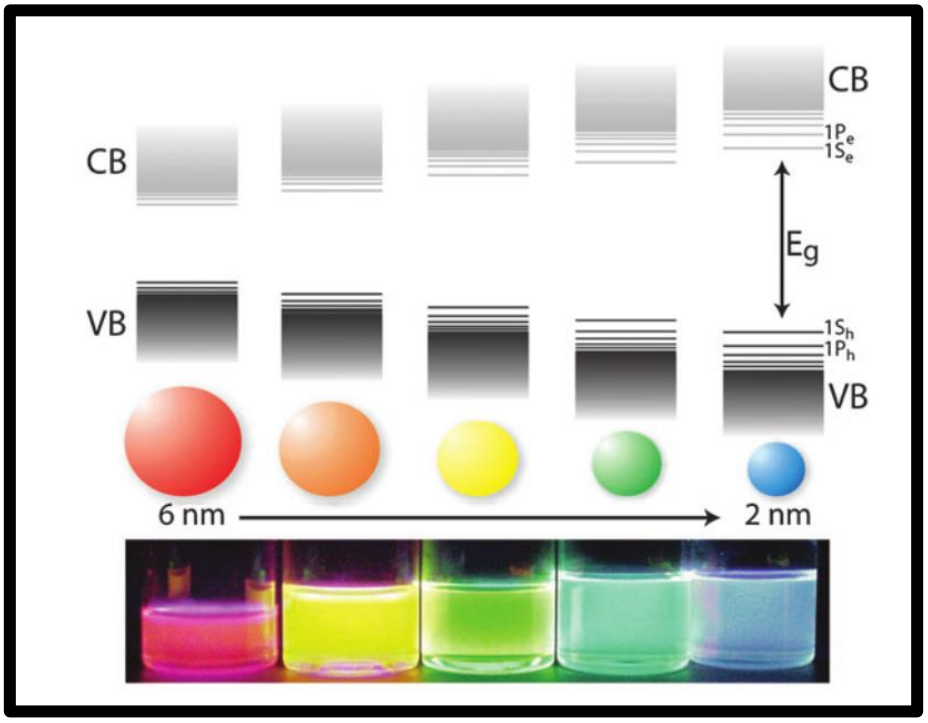

Figure 3. Schematic representation of quantum confinement effects. The band gap of a semiconductor increases as particle size decreases. Figure reproduced from Ref. 5

As mentioned above, PL qualities of QDs are due to the radiative recombination of excitons from band-edge states. These states compete with other radiative and non-radiative decay channels involving mid-gap electronic states associated with structural imperfections and dangling surface bonds.[25] The addition of a CdS shell improves the PL properties of the QDs by passivating surface bonds, reducing the amount of mid-gap electronic states, and preventing resonant energy transfer between QDs, which can occur when QDs are closely packed in assemblies, and leads to a considerable

reduction of photoluminescence quantum yield.[29] The shell is also necessary to chemically stabilize the CdSe cores that are prone to degradation effects such as oxidation. This is particularly important for this project, as the NC assemblies formed from these NCs are dispersed in aqueous solution and would be very susceptible to oxidation from water molecules. The choice of CdS as the shell material is important for two reasons. Firstly, it minimizes the formation of structural imperfections at the interface between the two materials because the difference in crystal structure between CdS and CdSe is small.[30] Secondly, CdS has a larger band gap than CdSe and the band edge states of CdSe are located between those of CdS. This is known as a type I heteronanocrystal and it means that excitons are confined to the CdSe core which prevents them from accessing mid-gap electronic states at the particle surface and helps to ensure radiative recombination occurs.

The NC surface is covered in capping ligands that passivate dangling surface bonds and ensure that the particles remain colloidally stable. The ligands are comprised of a polar head group that is bound to the particle surface and an apolar tail that extends from the particle surface out into the surrounding solution. Repulsive Van der Waals (VdW) interactions between ligands provides steric stabilization of NCs, which prevents aggregation due to interparticle attractions.[5] The apolar tail of the ligands ensures the NCs are dispersible in apolar solvents (Fig. 4).

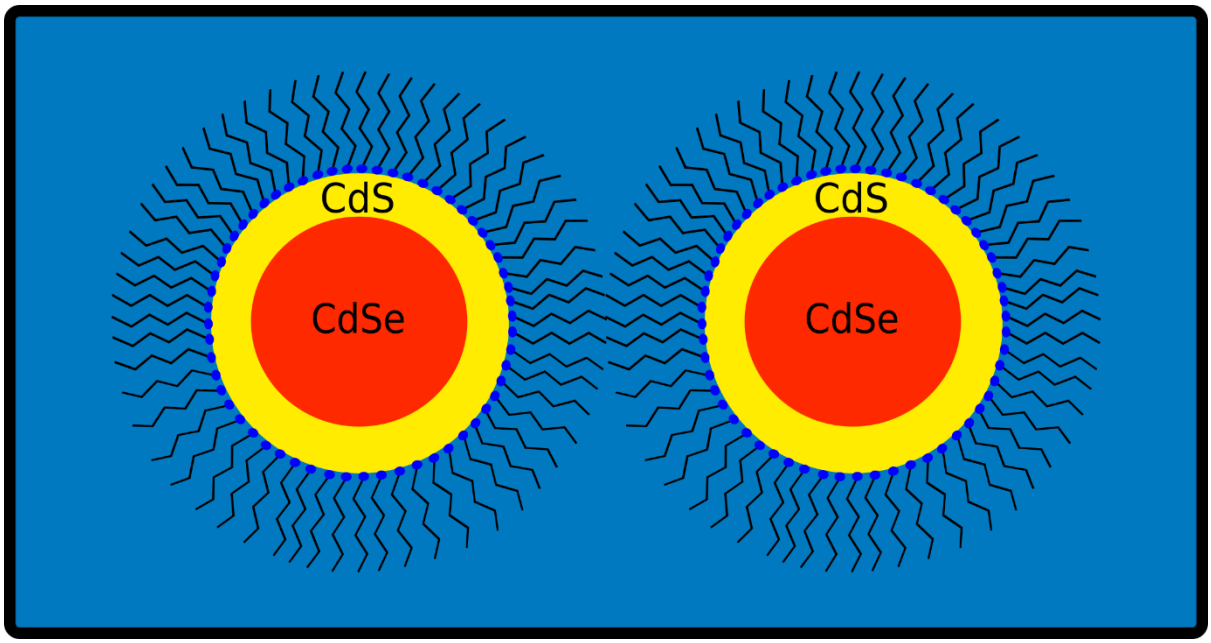

Figure 4. Schematic representation of core/shell NCs with surfaces sterically stabilised by ligands

Formation Mechanism

The underlying mechanism behind the formation of QDs in solution can be described by classical nucleation theory (CNT).[31] In CNT, a nucleus is formed from the bonding together of monomers, which are the individual atoms or molecules that make up a material. The thermodynamics of CNT are described by the total Gibbs free energy of a nucleus (eq.1)

$$\Delta G_{total} = \Delta G_s + \Delta G_v = 4\pi r^2\gamma - \frac{4}{3}\pi r^3 \frac{k_B T ln(S)}{v} \qquad (1)$$

Where ΔG_s is the contribution of the nucleus surface to the total Gibbs free energy, ΔG_v is the contribution of the bulk, r is the radius of the nucleus, γ is the interfacial tension, k_B is the Boltzmann constant, T is temperature, v is the molar volume of the semiconductor and S is the supersaturation of the solution. As the size of the nucleus increases, the surface contribution increases by a factor of

r^2 and the bulk contribution decreases by a factor of r^3. This leads to an initial increase in total Gibbs free energy for growing nuclei, presenting an energetic barrier to growth that causes small nuclei to redissolve. Due to the difference in scaling between the surface and bulk contributions, growth becomes thermodynamically favourable when the nucleus reaches a critical size (eq.2)

$$r_{critical} = \frac{2\gamma v}{k_B T ln(S)} \qquad (2)$$

Synthesis of low polydispersity samples of CdSe cores is achieved using the hot injection method. This method involves the rapid injection of one precursor into a hot coordinating solvent containing the other precursor.[5] Reaction kinetics allow the control of the size and polydispersity of the NCs produced and this is well described by the mechanism proposed by LaMer.[31] The process is divided into three steps, (1) Saturation, (2) Nucleation and (3) Growth (Fig.5). The saturation step is the quick injection of precursor that saturates the solution with monomers. When the concentration of monomers in solution exceeds a critical point, nucleation occurs. Nucleation lowers the concentration of monomers in solution below the critical point and nucleation stops. The polydispersity of the nuclei formed during this step controls the polydispersity of the final sample, so a fast nucleation step is important for ensuring the size distribution is low. The concentration is lowered below the critical point so no new nuclei are formed but the remaining monomers in solution add to the existing nuclei, causing them to grow.[32] The final size of NCs depends on the growth time. Growth is stopped by quenching the reaction by cooling or adding excess organic ligands.

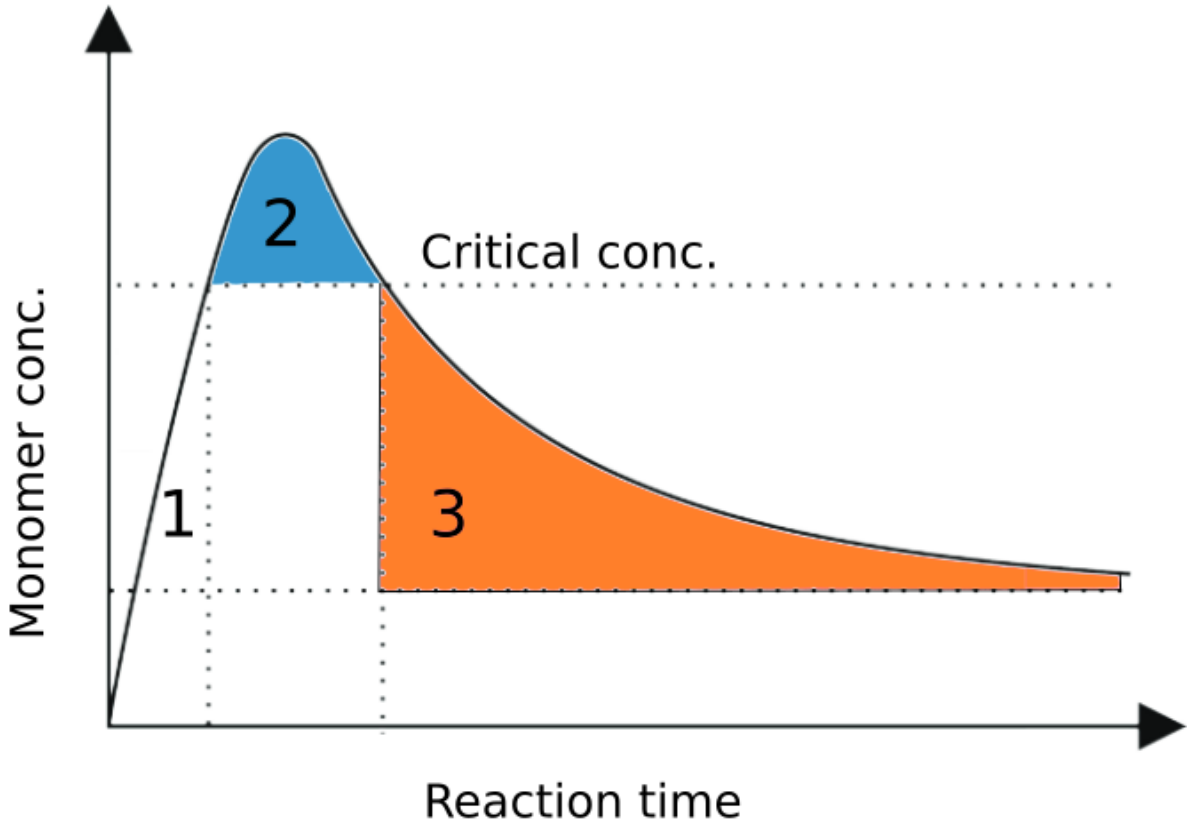

Figure 5. Plot outlining the kinetic model for formation of nuclei and growth of NCs

After the core particles are isolated from the reaction solution and washed, it is possible to determine their size and concentration from their absorption spectrum.[33] It is then possible to calculate the precise amount of shell precursors to add to obtain the desired shell thickness. The shell

addition done by adding the cores to a co-ordinating solvent, heating this solution to a desired reaction temperature and then gradually adding the calculated amount of each shell precursor.

Self-assembly of Colloidal Nanocrystals

Thermodynamics

Self-assembly is a spontaneous process that occurs because it reduces the Gibbs free energy of the system.[34] Equation 3 defines the change in Gibbs free energy of a system (ΔG) and for a process to occur spontaneously, Δ*G* must be less than zero. In the case of a solution of colloidal NCs, the enthalpy term (ΔH) accounts for the attractions between the nanocrystals in an assembly compared to those in the suspension and is assumed to be constant. The entropy term (Δ*S*) represents the degree of disorder in the system. The formation of NC assemblies corresponds to a negative Δ*S*, which according to classical chemical thermodynamics gives a positive value for Δ*G*, indicating that the process cannot proceed spontaneously.

$$\Delta G = \Delta H - T\Delta S \qquad (3)$$

Contrary to classical chemical thermodynamics, in the case of hard sphere colloids that have no attractive interactions, it is possible for the process to proceed spontaneously for a systems with a high volume fraction of NCs.[35,36] For hard sphere colloids, ΔH is zero and Δ*S* is positive for a crystal compared to a dense dispersion because the free volume per particle can be larger in an ordered crystal structure than in a chaotic dense dispersion for volume fractions above 0.5.[37]

$$\mu = \mu^* + k_b T \ln \frac{c}{c^*} \qquad (4)$$

In the case of hard sphere colloids, the chemical potential of the nanocrystals in suspension (eq. 4) helps to describe the self-organization into superlattices. One can view μ as the average free energy per NC. When the chemical potential of NCs in solution is increased, the NCs seek to find a lower energy state by organizing into crystals. The easiest ways to induce crystallization in this case is to increase the standard chemical potential (μ^*) by adding anti-solvent to the solution or by gradually increasing the concentration of NCs in solution (c) through the evaporation of the solvent. For this project we used the latter method. When trying to induce crystallization in this way, simulations have shown that, for a system of hard spheres, crystallization begins when the particles reach a volume fraction of 0.494 in solution.[38] Crystallization continues until the system reaches a final volume fraction of 0.740, which corresponds to the packing factor of an fcc lattice. This is because fcc packing has the lowest free energy for a system of hard spheres at equilibrium.[39]

When trying to create crystal structures based on the theory outlined above, ideally one wants the NCs used to behave according to the hard sphere model. This means that there are no attractive interactions between particles and particles only repel each other when they come into contact. This model has been applied to atomic and molecular systems to better understand the thermodynamics of phase transitions.[40] The same model can be applied to a system of colloidal NCs. Steric stabilization using organic ligands minimizes the interparticle attractive interactions. Their small size means they experience Brownian motion, which allows the system to explore the phase space of statistical mechanics meaning that the particles move around in such a way that they can minimize the systems free energy.[41]

Nanoscale Forces

In a system of colloidal NCs there are forces that can prevent the particles from behaving as hard spheres. Interparticle forces include electrostatic forces and VdW interactions. The method used for

this project involves a two-phase system with a liquid-liquid interface, so particles can experience attractive interactions with the interface and may also experience capillary forces if absorbed to the interface. It is worth noting that the forces only become significant if they have an energy greater than the thermal energy of the system, k_bT.

Electrostatic interaction can be attractive or repulsive depending on whether particles are similarly or oppositely charged. The influence of electrostatic interactions is minimized here because the NCs used have no net charge and their surfaces are passivated by organic ligands which also have no charge once bonded to the NCs.[42] VdW forces originate from electromagnetic fluctuations caused by the constant movement charges within atoms and molecules. VdW forces are present in all types of materials and can give rise to interactions, usually attractive, that are significant on the nanoscale.[43] The magnitude of VdW forces is dependent on the distance between interacting particles and there size. The magnitude scales with r^{-6}, where r is the distance between particles, and increases with particle size. In the case of semiconductor NCs these interactions can be effectively screened by the ligands used for steric stabilization as they maintain a distance between the NCs at which the forces are weak.[36]

The method used for this project involves the self-assembly of nanocrystals through spherical confinement in an oil-in-water emulsion. In this case, interaction of particle with the liquid-liquid interface can have a significant effect on the self-assembly process. The interfacial tension between the two phases, contributes to the total free energy of the system. The larger the surface area of the interface the greater the interfacial energy contribution to the total free energy. NCs dispersed in solution can adsorb to the interface because it reduces the surface area of the interface, lowering the total free energy of the system.[42] The change in interfacial energy for the absorption of an individual NC to the interface is given by equation 5.

$$\Delta E = -\frac{\pi r^2}{\gamma_{ow}}[\gamma_{ow} - (\gamma_{pw} - \gamma_{po})]^2 \qquad (5)$$

This change in energy is calculated using the interfacial tension values for the oil/water (γ_{ow}), particle/water (γ_{pw}) and particle/oil (γ_{po}) interfaces and r is the NC radius. If the energy decrease is greater than the thermal energy k_bT then particles will absorb to the interface.[44] From equation 5, it is clear that for a system of fixed temperature and interfacial tension values, the strength of absorption to the interface is dependent on particle size. For this reason, the change in energy for the absorption of NCs is small and usually of the order of k_bT. If absorption is favoured and the particle concentration is high enough, then either the interface will become saturated or the interfacial tension is lowered to a point where a dynamic equilibrium is reached and particles absorb and desorb at the same rate.[42]

When particles absorb to an interface, menisci can develop between them producing capillary forces that pull them together. These forces can cause irreversible aggregation of particles because once particles are pulled close enough together by capillary forces they are then held together by VdW attractions which only become very strong at small inter-particle distances.[45]

Our aim is to have particles that behave as hard spheres and so we must take measure to minimize the influence of these forces. Steric stabilization of the NCs is vital for this reason. The use of a surfactant to minimize the interfacial tension between the two liquid phases of the system can also help to prevent NCs adsorbing to the interface.[46,47]

Emulsion-based Self-assembly

This project employs a method which involves the self-assembly of NCs through spherical confinement in an oil-in-water emulsion.[19] An emulsion is formed when a mixture of two immiscible liquids is agitated, causing the less abundant phase to break in to droplets suspended in the other phase. In this case the liquid phase inside the droplets is called the dispersed phase and the surrounding liquid is the continuous phase. The presence of a surfactant at the interface lowers the interfacial tension between the two phases[47] and induces charging of the droplet surface, greatly increasing stability of the emulsion. We used the emulsion-based method because we are trying to produce monodisperse spherical assemblies that are suitable for hierarchical self-assembly. Other methods rely on the nucleation and crystallization occurring on a 2-D substrate or at an interface, which gives very little control over the shape of the assembly formed. The emulsion-based method confines the NCs in 3 dimensions and the spherical droplets provide a template for the shape of the final SPs.

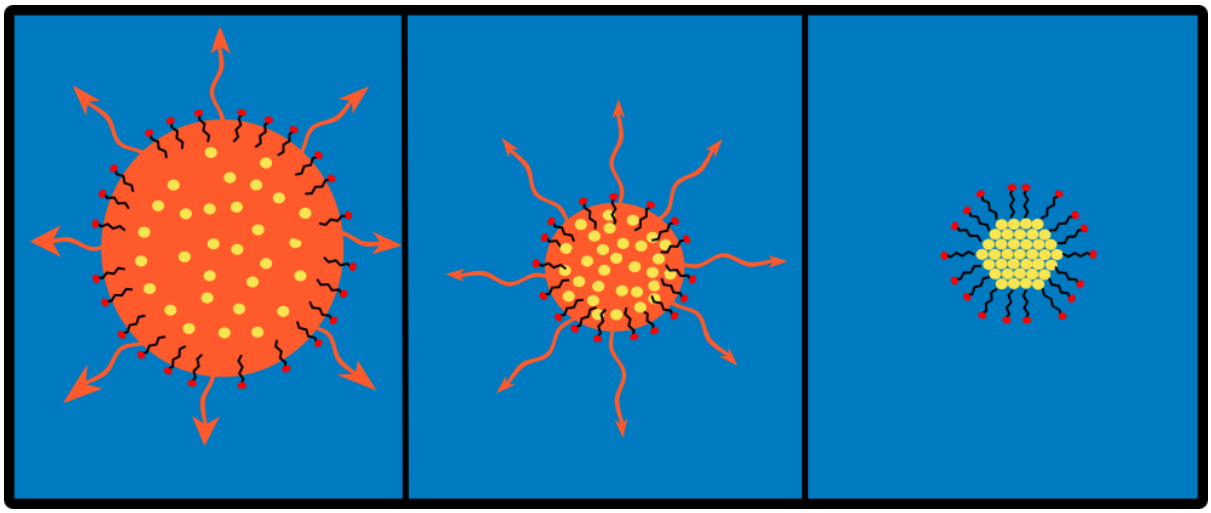

Figure 6. Schematic representation of the emulsion-based method for inducing the self-assembly of colloidal NCs. Dispersed phase droplet shrinks as organic solvent gradually transfers into the surrounding aqueous phase. The confinement of NCs induces the formation of a 3-dimensional assembly of NCs.

Emulsification in Viscoelastic Media

To form monodisperse SPs we will need to form monodisperse emulsion droplets. To achieve this, we need an emulsification method that provides controlled break-up of the dispersed phase into monodisperse droplets. When dealing with fluids it is important to consider the Reynolds number (eq.6) which is a value used to help predict flow patterns of fluids in particular situation. To ensure the droplet formation is consistent and controlled it is important that Reynolds numbers are low and laminar flow is exhibited.[48]

$$Re = \frac{\rho v L}{\eta_e} \qquad (6)$$

ρ is the density of the fluid, v is the velocity of the fluid, L is the diameter of the capillary and η_e is the dynamic viscosity of the fluid. For our experiments, dextran was added to the continuous phase to increase its viscosity and lower the Reynolds number. The capillary number(Ca) is defined as the ratio between the shear stress ($\eta_{eff}\sigma$) and the Laplace pressure (γ/r). For a droplet to form, the capillary number (eq.7), must exceed a critical value of order unity.

$$Ca = \frac{\eta_{eff}\sigma r}{\gamma} \qquad (7)$$

η_{eff} is the effective viscosity of the two phases, σ is the shear rate, r is the radius of the droplet and γ is the interfacial tension. In our case the shear rate is proportional to the ratio between the flow rates of the different phases. If we assume Ca to be 1 then the equation can be rearranged (eq.8) to highlight the influence of the different factors on droplet size.

$$r = \frac{\gamma}{\sigma \eta_{eff}} \qquad (8)$$

Emulsification Methods

To make SPs suitable for hierarchical self-assembly and the formation of a photonic crystal, the method used must have good control over size, shape and polydispersity. The polydispersity of the SPs formed from the emulsion is completely dependent on the initial size distribution of the emulsion droplets because the size of the droplet determines the number of NCs inside, which in turn determines the size of the SP formed. There are many ways of creating an emulsion, but the primary method used in this project uses a microfluidics technique that forms monodisperse droplets. The microfluidics devices are fabricated in-house. The key components of the device are three glass capillary tubes, each with a different diameter. The tubes are combined in such a way that allows the dispersed and continuous phases to be added through separate inlets. The phases combine inside the device, and droplets form due to shear stress exerted on the dispersed phase by the faster flowing continuous phase (Fig.7). The speed of the continuous phase flow relative to dispersed phase flow, determines the shear rate (σ). Emulsification using microfluidics produces monodisperse droplets, but it is time consuming because droplets are created one at a time. The size of the droplets produced can be adjusted by changing the shear rate but the sizes achievable are ultimately dependent on the device used. For the set-up we used for this project, droplet with diameter between 45-85µm were produced.

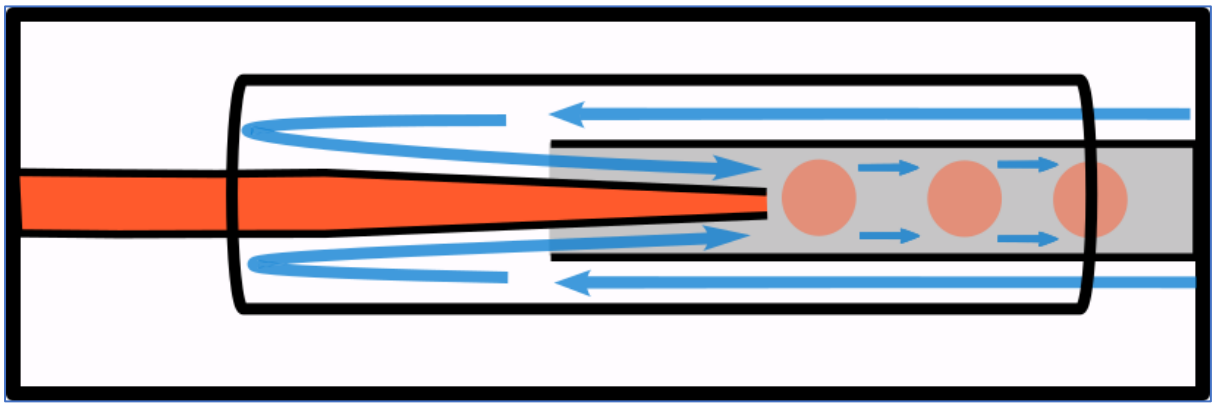

Figure 7. Schematic representation of the inner workings of the microfluidics devices used for this project. Aqueous continuous phase flows into outermost capillary. It then flows around the capillary containing the dispersed phase solution. Dispersed and continuous phases meet in the collecting capillary and dispersed phase is ruptured into droplets because of the shear force exerted by the faster flowing continuous phase.

We also used mechanical mixing using a Taylor-Couette shear cell to create emulsions.[49] The shear cell is a mechanical device that uses an inner spinning rotor inside a static outer cylinder. For this technique, the shear rate is proportional to the speed of the rotor and the characteristic length that determines the Reynolds number, corresponds to the spacing between the rotor and the outer cylinder. This technique produces droplets as small as 1µm and is much faster than using microfluidics, but the polydispersity of the droplets produced is significantly higher(~30%).

Sonication is also used as a method for producing emulsions during this project. An emulsion is formed by causing highly localised extreme pressure fluctuations in a mixture of two immiscible liquids .[50] It is a simple and fast technique, usually taking a few minutes to create an emulsion, and making droplets with diameters less than 1µm. The size of the droplets formed can be controlled by adjusting the amplitude and frequency used. More energy, or higher frequency, is required to make smaller droplets because smaller droplets means an increased number of droplets and an increase in interfacial surface area between the two phases.

Methods

In this section we outline the methods used for NC synthesis. We then show the method for the fabrication of the microfluidics device used. We then outline the methods used for SP assembly and finally we mention the characterization techniques used throughout the project.

List of chemicals

Chemical	Abbreviation	Supplier	Purity (%)
Selenium powder	Se powder	Alfa Aesar	99.999
Cadmium Oxide	CdO	Merck	>99
Cadmium Acetate	CdAc	Sigma-Aldrich	≥98
Sulfur powder		Alfa Aesar (puratronic)	99.999
Cobolt Chloride	$CoCl_2$	Merck	>99
Iron Chloride	$FeCl_3$	Sigma-Aldrich	≥98
Octadecylphosphonic Acid	ODPA	Sigma-Aldrich	97
Octanethiol	OT	Sigma-Aldrich	98.5
Oleic Acid	OA	Sigma-Aldrich	90
Oleyl Amine	OLAM	Sigma-Aldrich	70
Octadecylamine	ODA	Sigma-Aldrich	90
Trioctylphosphine	TOP	Sigma-Aldrich	90
Trioctylphosphine Oxide	TOPO	Sigma-Aldrich	90
1-Octadecene	ODE	Sigma-Aldrich	90
1-Hexadecene	HDE	Sigma-Aldrich	99
Cyclohexane		Arcos Organics	99.8
Hexane	Hex	Alfa Aesar	anhydrous
Heptane	Hept	Sigma-Aldrich	≥99
Toluene	Tol	Sigma-Aldrich	99.8
Dextran from leuconostoc mesenteroides (av.mol. wt 1,500,000-2,800,000)	Dex	Sigma-Aldrich	95
Methanol	MeOH	Sigma-Aldrich	99.8
Ethanol	EtOH	Alfa Aesar	94-96
Butanol	BuOH	Sigma-Aldrich	99.8
Sodium Hydroxide	NaOH	Sigma-Aldrich	≥97
Sodium Dodecyl Sulfate	SDS	Sigma-Aldrich	95

Table 1. List of chemicals used during the project and their abbreviations used.

CdSe synthesis

Two methods were used to synthesize the CdSe NC cores used for this project. The main difference between the two methods was the ligands used to stabilise the core particles. Method 1, following the procedure outlined in the paper by Li et al[28], produced core particles stabilised by TOP and OA whereas method 2, following the procedure used by Chen et al[27], made cores stabilised by TOP and ODPA, rendering them stable at higher temperatures compared to those synthesized by method 1.

Method 1

A 0.1M solution of cadmium precursor was prepared by dissolving 1.33g of $CdAc_2$ in 39.45g of ODE and 2.84g of OA. This mixture was degassed for 3hrs and stored in inert atmosphere glovebox. A 0.736M solution of selenium precursor was prepared by dissolving 1.42g of Se powder in 7.50g of TOP and 11.9g of ODE. 3.2g of ODA (previously degassed), 1.11g of TOPO (previously degassed) and 5.2g of selenium precursor was combined in a 50ml round bottom flask (RBF). 6ml of cadmium precursor was loaded into a syringe inside the glove box and removed. The RBF was attached to a shlenkline and put under vacuum. The reaction mixture was heated to 100°C. The RBF was put under nitrogen and the temperature was increased to 300°C. Cadmium precursor was swiftly injected, temperature was lowered to 280°C. After 7 minutes and the reaction was quenched by removing heat and cooling the reaction vessel with compressed air. The resulting particles were precipitated by adding a mixture of MeOH:BuOH (1:3). The particles were then isolated by centrifuging at 2750 RPM for 10 minutes. The clear supernatant was discarded, and the precipitate dispersed in Hex.

Method 2

Selenium precursor was prepared by dissolving 2.4g of Se powder in 20ml of TOP resulting in a 1.52M solution. To begin the synthesis, 60mg of CdO, 280mg of ODPA and 3g of TOPO were added to a 50ml RBF. This flask was connected to a shlenkline, then put under vacuum, heated to 150 °C and left to degas for 1hr. The reaction vessel was then put under nitrogen atmosphere and heated to 320 °C. The mixture was kept at this temperature until it formed a clear colourless solution. At this point 1ml of TOP was added to the solution and the temperature was increased to 380 °C. Se precursor was quickly injected and the reaction was quenched after a few seconds by removing heat and cooling the reaction vessel with compressed air. The resulting particles were precipitated by adding a mixture of MeOH:BuOH (1:3). The particles were then isolated by centrifuging at 2750 RPM for 10 minutes. The clear supernatant was discarded, and the precipitate dispersed in Hex.

CdS shell Growth

Precursor preparation

A 0.05M solution of Cd-oleate precursor was prepared by combining 1.33g of CdAc, 2.84g of OA and 39.45g of ODE in a 100ml RBF. The RBF was then connected to a shlenkline and put under vacuum gradually to avoid vigorous evaporation. The temperature was increased to 150 °C and the solution was left for 3hrs to completely degas. The RBF was then put under nitrogen, detached from the shlenkline and transferred to a glovebox where it was stored.

Two different sulphur precursors were used during this project. The first was simply a 0.1M solution of sulphur in ODE that was prepared in a glovebox by adding 0.032 g sulphur powder to 10ml previously degassed ODE and stirring at 120 °C to dissolve. The other precursor was a 0.12 M solution of OT in ODE that was also prepared in a glovebox by adding 0.625 ml of OT to 29.375 ml of degassed ODE.

Method 1: SILAR

This method for the shell addition was adapted from the method outlined in the paper by Li et al.[28] A typical synthesis was as follows. Inside a glovebox, CdSe nanocrystals (1×10^{-7} mol) dispersed in 2.66ml Hex were combined with 1.51g ODA and 6.0 ml ODE in a 20 ml glass vial. This mixture was heated to 150 °C and left for 1hr to evaporate the hexane. The temperature was raised to 250 °C and the 0.1M Cd-oleate and 0.1M S-ODE precursors were injected alternately at time intervals according to the scheme in table 2.

Precursor	Volume (ml)	Time (mins)
Cd	0.231	0
S	0.231	13
Cd	0.279	31
S	0.279	44
Cd	0.331	62
S	0.331	75
Cd	0.388	93
S	0.388	106

Table 2. Scheme outlining the volume and timing for injection of precursors during SILAR synthesis

Precursors are injected alternately to prevent both precursors being present in solution at once, causing the formation of independent CdS nanocrystals. After the last injection the solution was left to react for a further 15 minutes after which heating was removed and it was allowed to cool to room temperature. The reaction mixture was then diluted with hexane, the resulting particles were precipitated by adding MeOH:BuOH (1:3) mixture. The particles were then isolated by centrifuging at 3000 rpm for 10 minutes and the precipitate was redispersed in Hex.

Method 2: Continuous Addition

This alternative method for the addition of the CdS shell was taken from the same source as the synthesis method for the CdSe cores, the paper by Chen et al. [27] This paper claims that slow precursor infusion and the low reactivity of the OT precursor leads to a well maintained particle size distribution during the shell addition. The conditions that the synthesis took place under also ensured that the resulting QDs maintain the crystal structure of the CdSe cores.

To add 6 monolayers to 1×10^{-7} moles of CdSe cores, new precursor solutions were prepared by diluting the previously prepared ones with ODE. The concentrations of the resulting solutions were 0.031M and 0.0379M for Cd-oleate and OT respectively. The OT precursor solution was more concentrated due to its relatively low reactivity. CdSe nanocrystals (1×10^{-7} mol) dispersed in hexane were combined with 3 ml of ODE and 3 ml of OLAM in a 50 ml RBF producing a clear red coloured solution. The reaction vessel was then

connected to a shlenkline, put under vacuum and degassed at room temperature for 1 hr. The temperature was then raised to 120 °C and the mixture was degassed for a further 20 minutes. The reaction vessel was put under nitrogen atmosphere and syringes containing the precursor solutions were connected to the reaction vessel with capillary tubing inserted through a rubber septum. The temperature was gradually increased to 240 °C, at which point addition of precursors was initiated using a KD scientific LEGATO 111 syringe pump adding at a rate of 3 ml/hr. The temperature was increased until it reached 310 °C, where it was maintained until the remaining precursors had been added. After 6 ml of each precursor was added, 1 ml of OA was added, and the reaction was annealed at 310 °C for 1hr. The solution was allowed to cool to room temperature. The resulting particles were precipitated by adding MeOH:BuOH 1:3 mixture, isolated by centrifuging at 3000 rpm for 10 minutes and then redispersed in hexane.

Wüstite/Metal Ferrite Core/Shell Nanocrystal Synthesis

The method for the synthesis of metallic nanocrystals was based on that proposed by Bodnarchuk et al.[51] The NCs produced consist of a shell of $CoFe_2O_4$ surrounding a FeO core.

Precursor preparation

The precursor required for this synthesis was a mixture of Fe-oleate and Co-oleate with a 2:1 molar ratio. This was prepared by first dissolving 8.66 g of $FeCl_3 . 4H_2O$ (32 mmol) in 80 ml of MeOH and mixing it with 2.08 g of $CoCl_2$ (16 mmol) dissolved in 40 ml of MeOH. 5.12 g of NaOH dissolved in 320 ml of MeOH was added to the mixture over 45 minutes. The resulting brown viscous liquid was separated by decanting, washed 3 times with MeOH and dissolved in 80 ml of hexane. The hexane phase was separated using a separating funnel and washed three times using warm deionised water. The concentration was determined gravimetrically by drying a 1 ml aliquot of the solution. A precursor solution with a concentration of 0.5 mol kg^{-1} was prepared by adding 1.48 g HDE for each gram of mixed oleate. The hexane was removed by rotary evaporation at 30 °C.

Nanocrystal synthesis

9.6 g of mixed oleate precursor was mixed with 0.775 g OA and 13.736 g HDE in a 100 ml RBF. The resulting solution was black/brown and opaque. The reaction vessel was attached to a shlenkline via a condenser. The reaction vessel was put under vacuum and the mixture was degassed at 110 °C for 1hr. The reaction vessel was then put under nitrogen atmosphere and was gradually heated (2-4 °C min^{-1}) until it began to reflux at 295 °C. After refluxing for 35 minutes, heat was removed, and the solution was allowed to cool to room temperature. The solution was then mixed with 1 equivalent of a Hex-EtOH mixture and centrifuged at 4000rpm for 2 hrs. The precipitate was redispersed in cyclohexane.

Fabrication of Microfluidics Chips

The microfluidics chips used to create emulsions during this project were fabricated in house, following a method proposed by Haase.[52] The method involves combining three glass capillaries of varying sizes by inserting them inside one another and enclosing them using needles and glue. This section goes through the fabrication process step by step.

1. Paperclips were attached to either end of a 50 µm diameter glass capillary and it was hung from a clamp. A handheld Bunsen burner was used to taper the glass capillary by passing the flame quickly over the middle of the capillary. As the glass heats up, the weight of the paperclip pulls the lower half of the capillary down, stretching the glass and causing the capillary to narrow in the middle. The tapering of the capillary was confirmed by viewing it under a microscope
2. The capillary was carefully cut in half using a Molex cleaving stone and checked using a Leica DM IL LED microscope, to see if the cut was clean and didn't leave any jagged edges or chips of glass blocking the capillary.
3. The outer capillary (200 µm diameter) was cut to the desired size and attached to a glass microscope slide using glue. The glue was applied at points close to either end of the capillary but left adequate space for needle connections to be placed at either end.
4. A 100 µm diameter capillary was inserted into one end of the 200 µm capillary and the tapered end of the 50 µm capillary was inserted in to the other end. Both capillaries had one end inserted and the other end extruding from the outer capillary so that it was possible to manipulate them. Next, by viewing under a microscope, the 50 µm capillary was inserted into the 100 µm capillary while inside the outer capillary, as shown in Fig. 1. Both were then glued in place on the microscope slide, again leaving space for needle connections at either end.

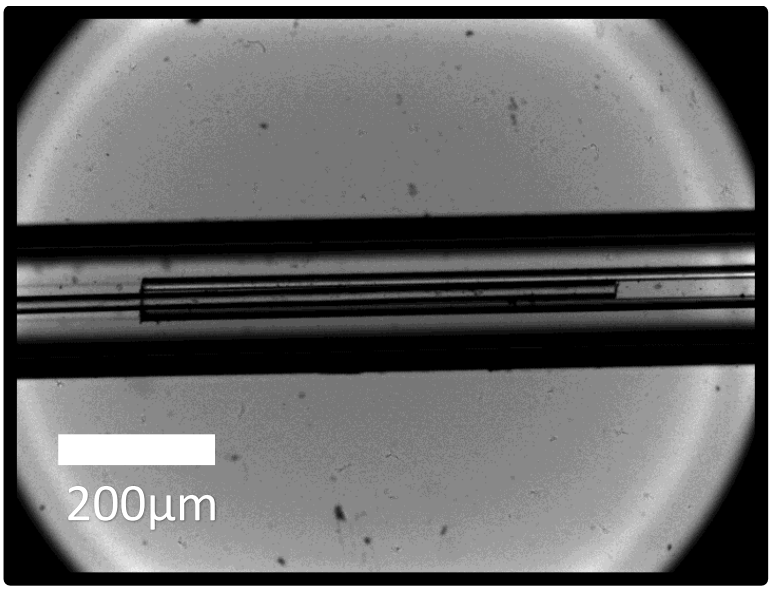

Figure 8 Microscope image of 50 µm capillary inserted inside 100 µm capillary, both inside the outer 200µm capillary.

5. After the glue had dried, the ends of both capillaries were cut to the desired size, leaving space at the end to attach the metallic connections to the microscope slide.
6. Two metallic connections were made from 0.8 mm diameter needles by breaking off the plastic syringe connector and bending the needle by 90°. The ends of both inner

glass capillaries were inserted into the sharp ends of the metallic connections, which were then glued into place on the microscope slide.

7. The needle connections were made by cutting small slices out of the plastic parts of the 0.8 mm needles so that they could be placed flat on the microscope slide at the points where the inner capillaries exit the outer capillary. These connections were glued in place
8. All connections were then covered in glue to fully enclose the capillaries and prevent any liquid from escaping from any gaps between the connections.

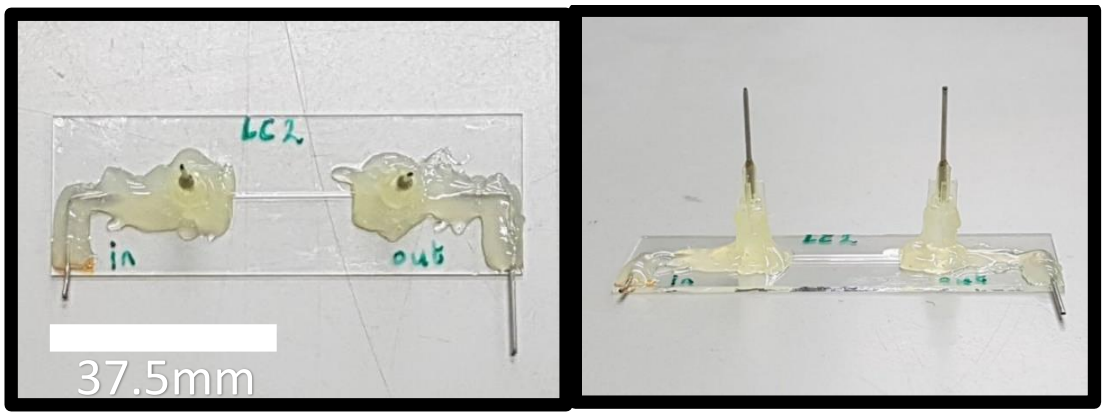

Figure 9 Images of the microfluidics chip after fabrication process is complete.

Supraparticle self-assembly

Dispersed phase preparation

The concentration of the NC containing dispersed phase was determined gravimetrically. In a typical case, a glass vial was weighed using an analytical balance. A few millilitres of NC stock solution were added to the pre-weighed glass vial. NCs were precipitated by adding a few millilitres of MeOH:BuOH (1:3) mixture and isolated by centrifuging at 2750 RPM for 10 minutes. The clear colourless supernatant was discarded, and the glass vial was placed in a vacuum chamber for 15 – 30 minutes to fully dry the precipitated particles. The vial was then re-weighed to determine the mass of the particles present. The mass was then used to find the number of particles present by dividing by the mass of a single particle, which was calculated based on mean size and bulk material density figures. The particles were then redispersed in the required amount of organic solvent to give the desired concentration.

Microfluidics

For a typical microfluidics based self-assembly experiment, 1 mg of 7.5 nm CdSe/CdS core/shell nanocrystals were dispersed in 1 ml of cyclohexane to produce the dispersed phase solution. The continuous phase was produced by dissolving 4 g of Dex and 0.6 g of SDS in 100 ml of deionised water. Both phases were loaded in to separate syringes and attached to the microfluidics chip using capillary tubing. Both phases were simultaneously injected using a Cetoni nemesys 290N syringe pump, with flow rates of 250 µl/hr for the dispersed phase and 2500 µl/hr for the continuous phase. The initial size of droplets was observed using a Leica DM IL LED optical microscope and images were captured using a Phantom Miro eX4 camera.

After 4 hrs, the collected droplets were dispersed in 5 ml of continuous phase and placed on a stirring platform to ensure the droplets remained dispersed. The emulsion was light orange coloured and turbid. After about 11hrs the evaporation was complete as turbidity had completely disappeared. The SPs produced were washed by centrifuging the solution at 2500 RPM for 10 minutes, removing supernatant using a pipette and redispersing in 1 ml of deionised water.

Taylor-Couette Shear Cell

The method for this technique was adapted from that proposed by Bibette et al.[53] 3.9 mg of 7.5 nm CdSe/CdS core/shell nanocrystals were dispersed in 0.5 ml of cyclohexane. This was combined with 5 ml of continuous phase solution and mixed by shaking. This mixture was transferred to a syringe and injected into the shear cell with a rotor speed of 7600 rpm and a gap spacing of 100 µm. The resulting emulsion was collected in a vial and then transferred to an oil bath that was kept at a temperature of 68 °C. To keep the droplets dispersed, the emulsion was stirred using a stir bar. After 6 hrs the vial was removed, and the SPs produced were washed by centrifuging the solution at 2500 RPM for 10 minutes, removing supernatant using a pipette and redispersing in 1 ml of deionised water.

Sonication

16 mg of 7.5 nm CdSe/CdS core/shell nanocrystals were dispersed in 1 ml of cyclohexane. The continuous phase was produced by dissolving 12.5 mg of SDS in 5 ml of deionised water. These solutions were mixed by vigorous stirring. The mixture was then sonicated for 30 seconds, mixed again by stirring and then sonicated again for a further 30 seconds. For high power sonication a Sonics Vibracell was used with a probe model CV33 at an amplitude of 23%. For low power sonication a Branson 8510 sonic bath was used. The emulsion was placed on a stirring platform to ensure the droplets remained dispersed. After about 11hrs the evaporation was complete as turbidity had completely disappeared. Washing was not needed because Dex was not used in the continuous phase.

Characterization

UV-Vis Spectroscopy

Absorption and emission spectra of CdSe and CdSe/CdS particles were measured. A Perkin Elmer Lambda 950 UV-Vis spectrometer was used to obtain absorption measurements. The emission spectra of samples were measured under illumination from a 395nm laser using an ocean optics USB4000 UV-Vis detector. Typically, 2 ml of organic solvent was added to 50 µl of stock solution in a 10mm quartz cuvette. A background spectrum was taken for absorption measurements. Spectra were measured in range of 400nm – 700nm.

Transmission Electron Microscopy

A Tecnai 20 electron microscope was used for analysis of both NC and SP samples. Depending on the concentration of the stock solution, NC samples were prepared by diluting the stock solution by 10 – 20 times and drop-casting 10 µl on to a copper TEM grid. Similarly, SP samples were diluted by 2 – 5 times ,depending on concentration, and drop cast in the same way.

Scanning Electron Microscopy

SP samples were analysed using a Phenom ProX scanning electron microscope. Samples were prepared by drop-casting 10 µl of SP solution on to a piece of silicon wafer and allowing the water to evaporate at room temperature.

Optical Microscopy

A Leica DM IL LED microscope was used during the fabrication of microfluidics chips and to observe the droplets produced by microfluidics. Images from the camera were captured using a Phantom Miro camera.

Results and Discussion

This section reviews the results obtained from our experiments. First, we looked at sizes, polydispersity's and optical properties of the NC samples synthesized. This allowed us to determine if there is a distinction between the two synthesis methods used, and if the NCs are suitable for self-assembly. Next, we looked at the droplets produced by our microfluidics set up, observing the size and polydispersity. We also investigated how droplet size could be tuned by variation of continuous phase flow rate.

We show SPs formed from an emulsion made by mechanical mixing using a Taylor-Coutte shear cell. This was a much quicker technique, compared to microfluidics and so it was used to confirm that the NCs produced were capable of forming crystalline SPs, before moving on to using microfluidics. Next, we show the SPs formed from emulsions made using our microfluidics set up. In our attempts to reduce the size of the SPs formed using microfluidics, we observed the emergence of flaws and irregularities on SP surfaces. To understand the reasons for this and improve the SP surfaces, we investigated changing the evaporation time, temperature and solvent used during SP formation. We also looked at SPs formed from emulsions made using sonication. Emulsions made using sonication have much smaller droplet sizes than the emulsions we made using microfluidics, so this enabled us to form SPs of similar size to those formed using microfluidics, but by using a dispersed phase solution with a much higher concentration of NCs. The experiments done with sonication allowed us to investigate the effects of initial dispersed phase concentration on SP formation.

Nanocrystal Characterization

CdSe Core characterization

The size dependent band gap of CdSe quantum dots allowed us to determine the size of CdSe core particles from their absorption spectra. Using values gathered from litetrature[54,55], Yu et al[33] created a sizing curve (Fig.10A) by plotting the position of the first excitonic peak of the absorption spectrum against particle size and fitting a curve using an empirical fitting function (eq.9).

$$D = (1.6122 \times 10^{-9})\lambda^4 - (2.6575 \times 10^{-6})\lambda^3 + (1.6242 \times 10^{-3})\lambda^2 - (0.4277)\lambda + (41.57) \quad (9)$$

where D is the size of a given particle and λ is the wavelength corresponding to the first excitonic peak of the absorption spectrum. The position of the first excitonic peak corresponds to the wavelength of the photons that promote electrons from the band edge states in the valence band to the conduction band. The energy of these photons is equivalent to the energy of the NC band gap, which changes with

NC size due to quantum confinement. For this reason, the 1st excitonic peak is used to determine NC size. The sizing curve (Fig10A) was used to estimate the size of core particles using the peak position. The absorption spectra for the samples produced are shown (Fig.10B). The details of all the samples produced are shown in table 1. Samples labelled with 1 were synthesized according to the method outlined by Li et al[28], from here on referred to as method 1. These samples were synthesized at 300°C and were stabilised by OA. Samples labelled with 2 were synthesized according to the method outlined by Chen et al[27], from here on referred to as method 2. These samples were synthesized at 380°C and were stabilised by ODPA.

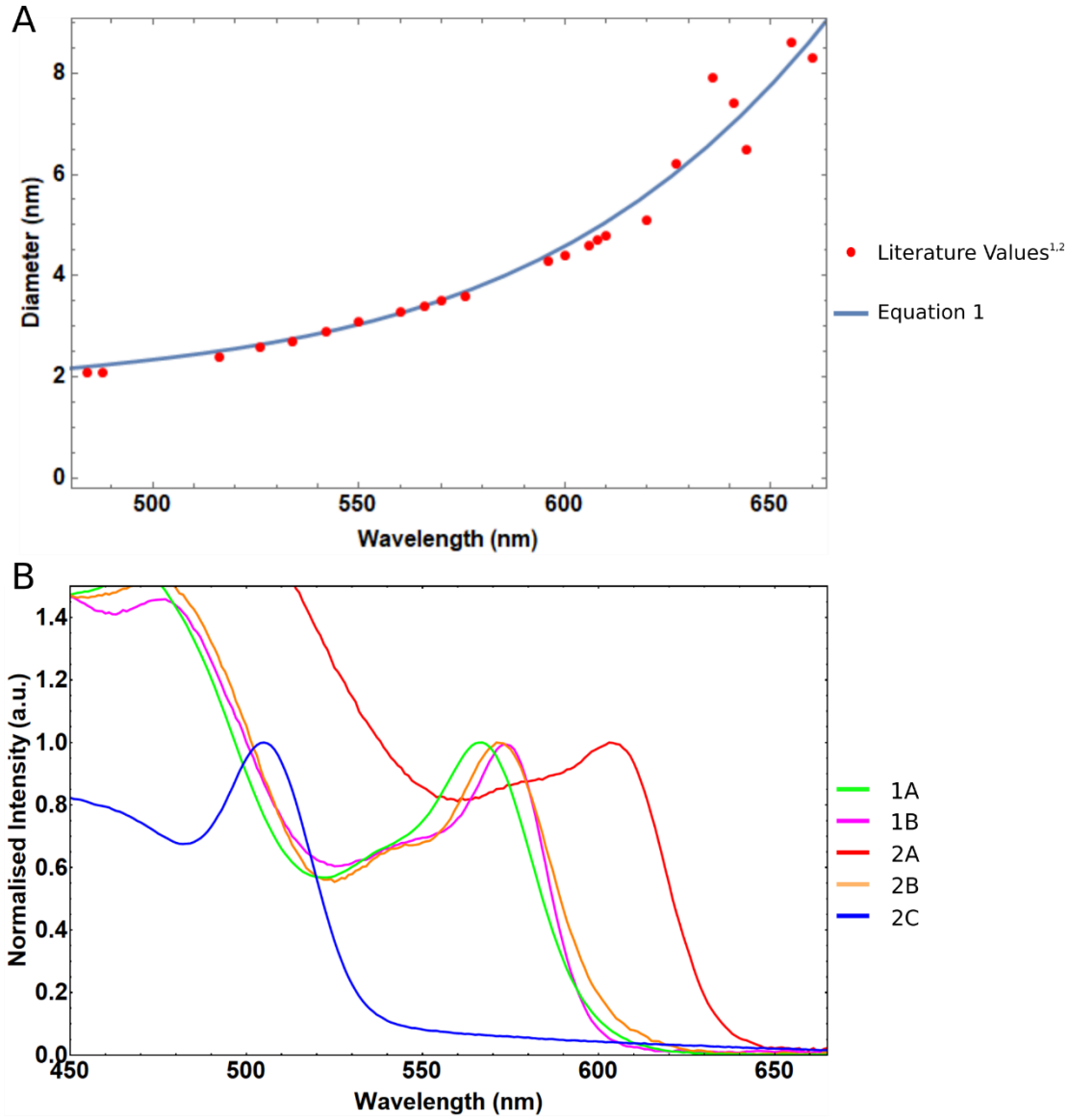

Figure 10 (A) Sizing curve for CdSe core particles.[33] (B) Normalised absorption spectra of CdSe samples

Sample	1st Excitonic Peak (nm)	Size (nm)	Emission peak (eV)	FWHM (eV)
1A	567	3.44	2.132	0.1134
1B	571	3.54	2.105	0.1133
2A	603	2.41	2.388	0.1511
2B	582	3.59	2.130	0.1018
2C	505	4.55	2.022	0.0999

Table 3. Details of all CdSe core nanocrystals samples synthesized. The number in the sample name denotes the synthesis method used as outlined in the methods section. Size listed was calculated using the sizing curve (Fig.1B).

The photoluminescent spectrum of CdSe QDs exhibits a stokes shift corresponding to an emission spectrum peak that is red shifted from the 1st excitonic peak of the absorption spectrum (Fig.11A).

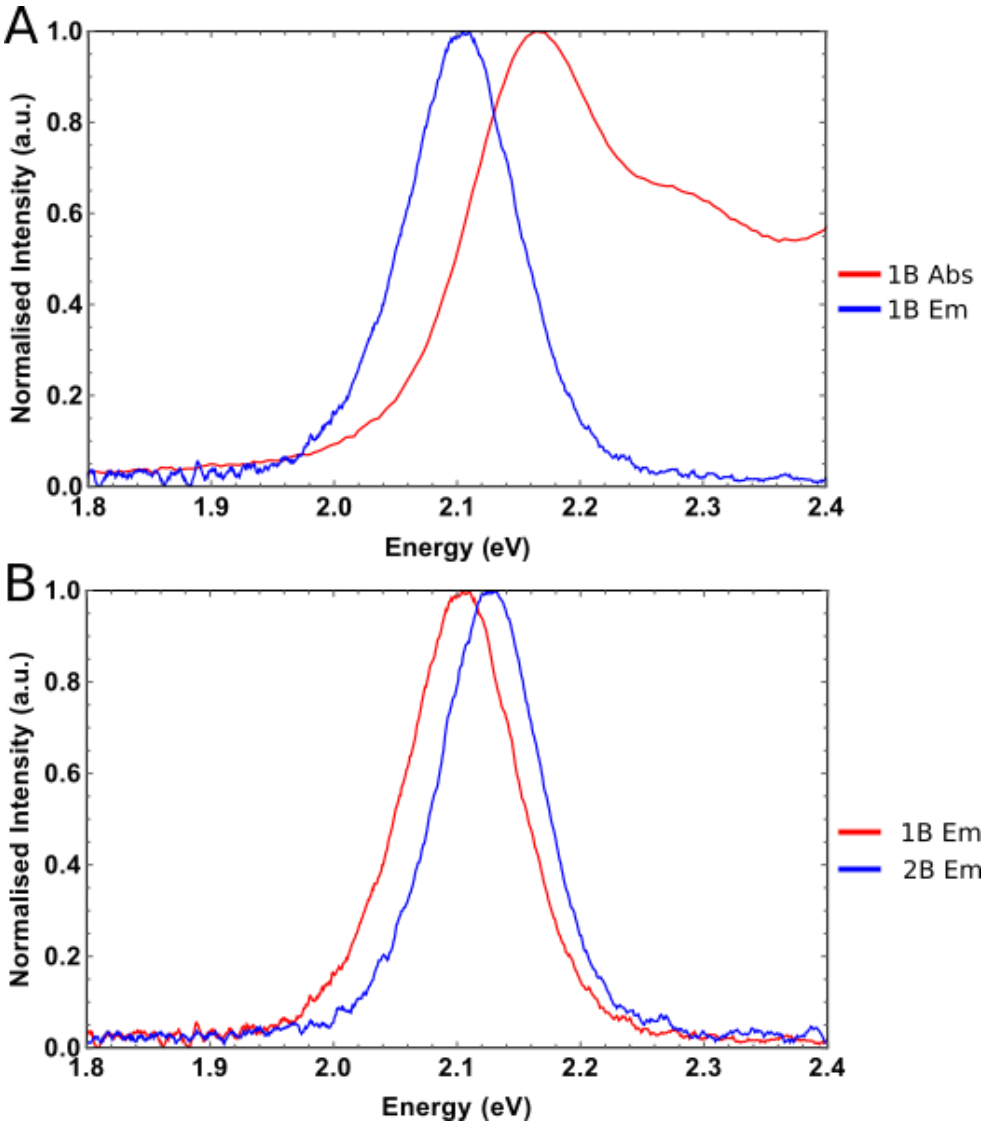

Figure 11. (A) Absorption and emission spectra of sample 1B. (B) Emission spectra of samples 1B and 2B

The full width at half maximum (FWHM) of emission spectra peaks were used as a measure of polydispersity for the core samples produced. The FWHM is indicative of the size distribution due to inhomogeneous contributions to the broadening of the emission peak. The ensemble emission peak of a sample broadens with increasing polydispersity.[56] Broadening of the emission peak can also be caused by coupling with longitudinal optical (LO) phonons.[56] This coupling is affected by particle size and therefore it is only appropriate to use the FWHM to compare the polydispersity for samples with similar sizes. Samples 1B and 2B are close enough in size that the peak broadening due to coupling with LO phonons is insignificant. Their FWHM were compared (Fig.11B) to determine which method produced samples of lower polydispersity. The FWHM of sample 2B is narrower by 11.5meV, indicating a narrower size distribution was obtained when using method 2. This could be explained by the short nucleation and growth time of method 2 compared to method 1. For method 2, the reaction was carried out at a higher temperature, so the reactivity of the monomers is higher, causing nucleation and growth of NCs to happen quicker.[32] The faster nucleation ensures good separation of

nucleation and growth phases, which is vital for producing a monodisperse sample. The reaction is quenched after a few seconds for method 2, which is very quick compared to the 7 minutes of growth time for method 1. The shorter time period for growth means there is a lower chance of the size distribution broadening by Ostwald ripening.[54]

Core/Shell Nanocrystal Characterization

CdSe/CdS core/shell QDs were synthesized by successive ionic layer adsorption and reaction method (SILAR), and continuous addition method (CA), which are both described in detail in the methods section. A significant difference between the methods is the Sulfur precursor used. The SILAR method simply uses a solution of sulphur powder dissolved in ODE. The CA method uses OT diluted with ODE. OT is less reactive due to the strong carbon-sulphur bond, so the CA reaction is carried out at the higher temperature of 310°C, compared to 250°C for the SILAR. The CA method uses the CdSe cores synthesized by method 1 because they were synthesized at 380°C, so they can remain stable when exposed to high temperature for a long time during the shell growth.

Low polydispersity samples are necessary for the formation crystalline SPs.[57] For an assembly to be crystalline it must be densely packed and its structure must have long range order. Polydispersity limits how densely the components of the crystal can be packed and leads to defects in the ordered structure.[45] Size and polydispersity of core/shell samples was measured through the analysis of TEM images (Fig.12). ITEM software was used to measure the size of 100 randomly selected NCs. Polydispersity was then calculated by dividing the standard deviation by the mean size and multiplying by one hundred to give a percentage. The results of this analysis are shown below (Table 4). This analysis shows that the CdSe/CdS samples synthesized by CA have a lower polydispersity than the sample made using SILAR. The reason for the lower polydispersity of the CA sample may be explained by the low reactivity of the OT sulphur precursor used, which ensures a slow and controlled shell growth. The authors of the paper outlining the method also claim that this controlled shell growth creates NCs with higher crystallinity relative to other methods.[27] This higher crystallinity may explain the more widespread ordered hexagonal packing of CA samples, compared to the SILAR sample, when they are deposited on a TEM grid (Fig.12 A,B,C). This is because, at the NC surface, there is a higher ligand density on the flat defined crystal facets compared to the corners or edges of these facets. This causes NCs to orient relative to each other in an ordered fashion.[58]

From these results it is clear that the QD samples synthesized using the CA method are more suitable for self-assembly because of their lower polydispersity and the fact that they spontaneously self-assemble into ordered monolayers when deposited on TEM grids. The $FeO/CoFe_2O_4$ sample has a significantly lower polydispersity compared to QD samples due to the reliable thermal decomposition synthesis mehtod.[51] They also spontaneously form ordered monolayers when deposited on a TEM grid (Fig.12D)

Sample	Count	Mean Diameter (nm)	Standard Dev.	Polydispersity (%)
SILAR 1B	101	6.65	1.03	15.5
CA 2A	100	7.52	0.81	10.7
CA 2B	100	8.55	1.02	11.9
$FeO/CoFe_2O_4$	82	8.72	0.51	5.8

Table 4. Data obtained from analysis of TEM images. CdSe/CdS sample names contain shell growth method and core sample used.

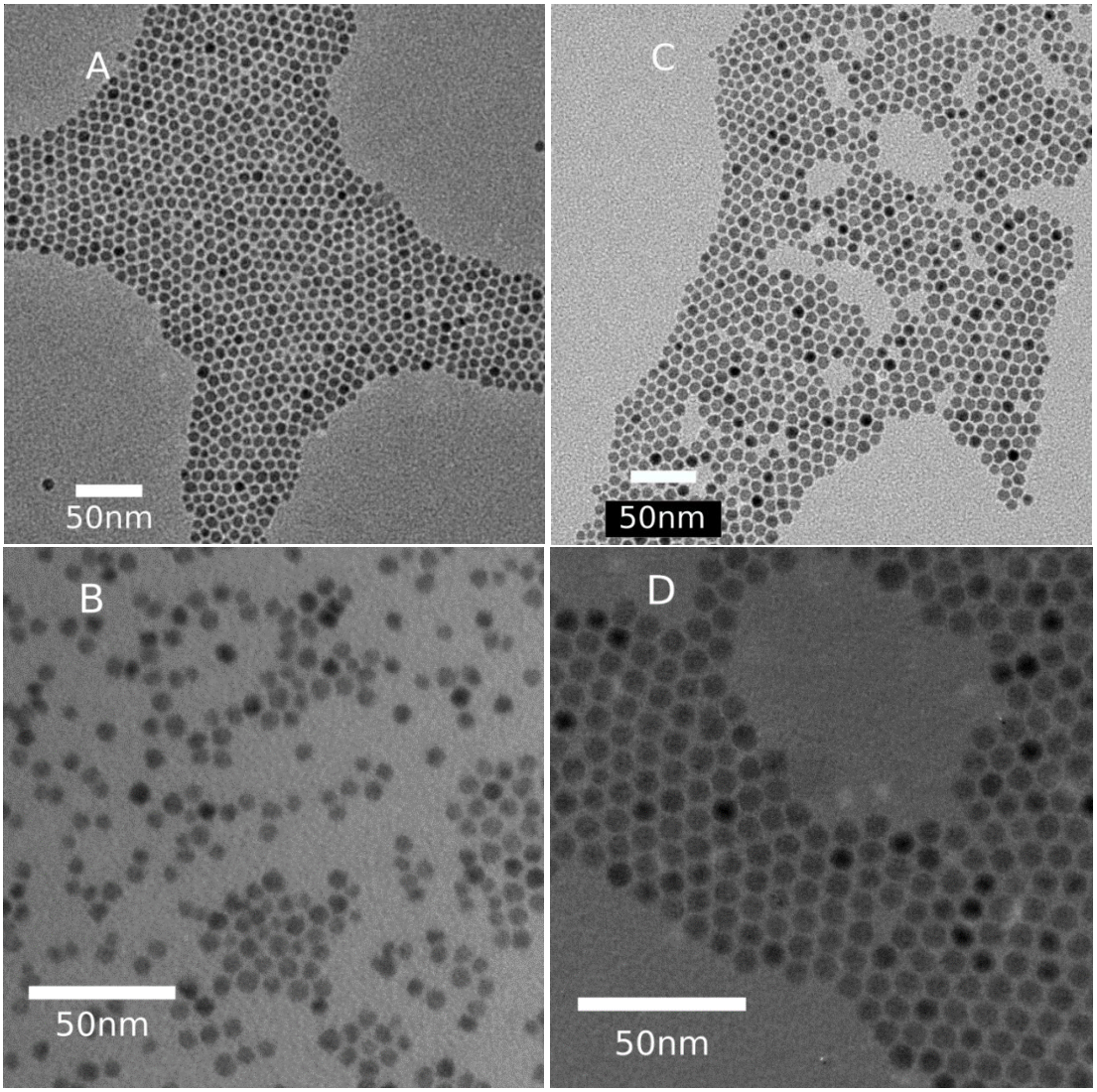

Figure 12. TEM images of CdSe/CdS particles synthesized by continuous addition method (A,C), CdSe/CdS particles synthesized by SILAR method (B) and FeO/$CoFe_2O_4$ NCs (D)

Supraparticles : Shear Cell as Emulsification Technique

The next step in the project was to use our previously synthesized NCs to form monodisperse SPs. For the first attempt at forming SPs, the emulsification method used was mechanical mixing using the Taylor-Coutte shear cell. In the work by De Nijs et al[59], this method has been shown to successfully produce SPs. However, the polydispersity of the droplets produced by this emulsification method contributes to broadening of the size distribution of the SPs formed. We require SPs samples with low polydispersity for hierarchical self-assembly, so this method was primarily used as a quick and easy way to confirm if the NC sample was capable of forming crystalline structure, before moving on to the more time-consuming microfluidics method.

The process was carried out as outlined in the methods section, using a 7.8 mg/ml solution of QDs (7.5nm) in cyclohexane as the dispersed phase. TEM and STEM were used to observe the SPs formed and ITEM software was used to measure the size and polydispersity. The mean diameter of the SPs formed was 355nm and polydispersity was 30%. The images are also used to observe whether or not individual SPs were crystalline. From the TEM images it is clear that at least partially crystalline structures are formed (Fig.13A,B). It is not possible to judge anything about the internal structure of the larger SPs because electrons are not transmitted all the way through, but near the edges of large

SPs and for smaller SPs electrons are transmitted and lattice planes are clearly visible. The STEM images show that the SPs vary between partially and fully crystalline. A high-angle annular dark field STEM image clearly show the internal crystallinity of the SPs as lattice planes are visible (Fig.13D). A secondary electron STEM image shows the ordered surface of the SP (Fig.13C)

The formation of a photonic crystal through SP self-assembly requires an SP sample with low polydispersity because polydispersity limits how densely the components of the crystal can be packed and leads to defects in the ordered structure. Polydispersity of 30% is very high, so this sample is considered unsuitable for hierarchical self-assembly. The crystallinity observed in the STEM images confirms that the NC sample is capable of forming crystalline SP but a new different emulsification method is required to produce an SP sample with lower polydispersity.

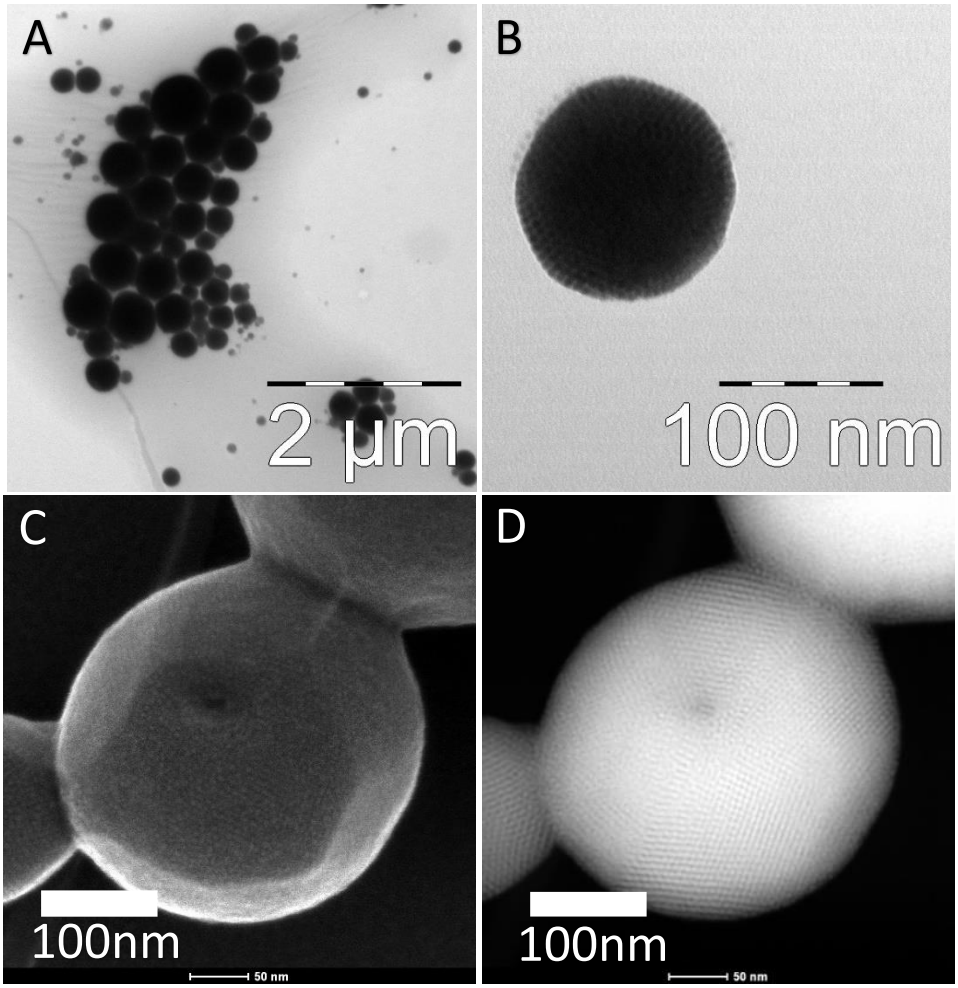

Figure 13. TEM (A,B) and STEM (C,D) images of SPs formed using shear cell as emulsification technique

Microfluidics: Droplet Size Control

To form a photonic crystal by self-assembly of colloidal SPs, we need monodisperse SPs. Since we are using an emulsion-based method for the formation of SPs, the size distribution of the emulsion droplets is directly related to the size distribution of the SPs formed. To achieve monodisperse SPs we need an emulsification technique that makes monodisperse droplets. Microfluidics techniques allow precise control and manipulation of fluids on the micrometer scale, so we investigated the use of microfluidics to make emulsions for SP formation. Making emulsions using microfluidics was carried out using our in-house fabricated microfluidics chips that were introduced in the methods section. The microfluidics chip was made from a 50µm glass capillary inside a 100µm capillary, both inside a

200µm outer capillary. The dispersed phase flows into the device through the 50µm capillary and the continuous phase flows in through the 200µm capillary. The two phases combine in the 100µm capillary and the dispersed phase in broken into droplets due to the shear force exerted on it by the faster flowing continuous phase.[60–62]

We investigated the effect of varying flow rate of the continuous phase on droplet size when using our in-house fabricated microfluidics chip to create an emulsion. We used cyclohexane as the dispersed phase and H_2O-SDS-Dex as the continuous phase. The droplets produced were on the µm scale, so it was possible to view them using an optical microscope. Figure 14D shows the plot of flow rate ratio vs droplet size and the microscope images of droplets collected at different flow rates. The reduction in droplet size is almost linear with increasing continuous phase flow rate. These results show that the droplet diameter can be tuned within the range of 85-44 µm using this microfluidics device. The droplet polydispersity was calculated at each flow rate. The highest polydispersity measured was 3.3%, which demonstrates the exceptionally low size distribution of the droplets produced. The small size distribution is achieved because droplets are formed one at a time, but this also makes the technique much more time consuming. For a typical SP experiment, droplets were collected for 4hrs to obtain 1ml of droplets.

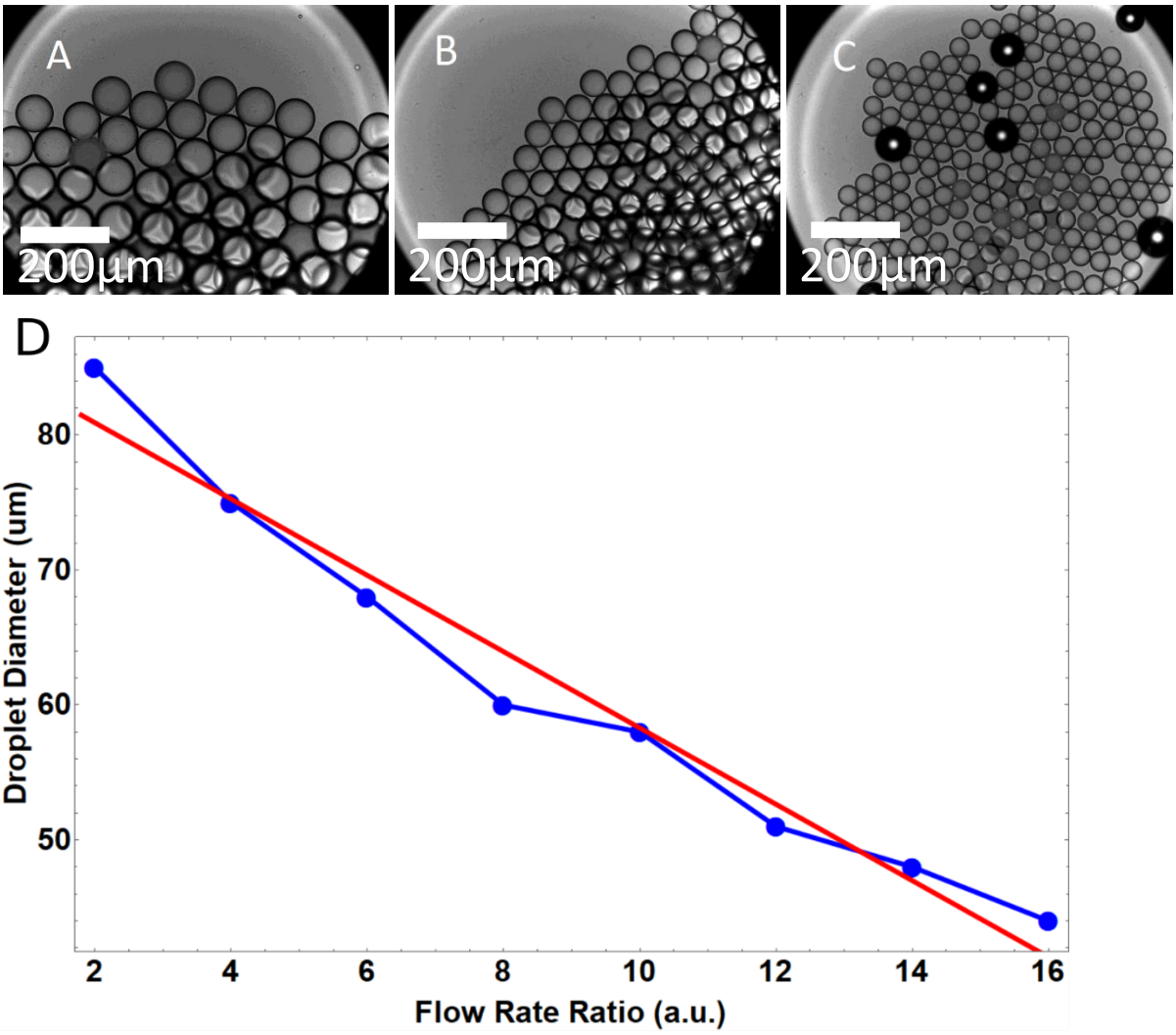

Figure 14. Optical microscope images of 85um (A), 60um (B) and 44um (C) droplets. Plot showing data (blue) and linear model fit (red) for droplet size plotted against ratio between flow rates of continuous and dispersed phases (D)

Supraparticles: Microfluidics as Emulsification Technique

In this section we show the results from our attempts to form SPs using microfluidics as the emulsification technique. Microfluidics is a promising technique for this application because it has the potential to produce monodisperse droplets, which we hope can help to form monodisperse SPs. The experiments in this section were carried out as outlined in the methods section and unless otherwise specified, the dispersed phase solution used was CdSe/CdS QDs in cyclohexane and initial droplet diameter was in the range of 58-64 µm. Our initial attempt produced a promising sample but the SPs were far too big to form a photonic crystal. To form SPs of the desired size we lowered the concentration of the dispersed phase. This negatively affected the quality of the SPs formed so we investigated changing multiple parameters such as temperature, evaporation time and nanocrystal solvent to see if we could control the quality of the SPs formed.

Initial Synthesis

For the initial attempt at using microfluidics for SP formation, we used a dispersed phase with a concentration of 10 mg/ml. Droplets were collected and dispersed in 5 ml of continuous phase solution in a small glass vial. vial was placed on a stirring platform to keep droplets dispersed in continuous phase. After 12 hrs, evaporation was complete. The resulting SPs were observed using SEM. From analysis of SEM images(Fig.15), we measured a polydispersity of 4% and mean diameter of 10.2 µm. The polydispersity 4% is a huge improvement from the polydispersity of 30% for the sample made using the shear cell, clearly showing the benefits of using microfluidics. Some of the SPs deposited on the silicon wafer formed regions of ordered hexagonal packing, clearly demonstrating the benefits of low polydispersity. The average size of 10.2 µm means that the particles are not colloidally stable. This means that they do not experience Brownian motion, so they settle out of solution when left undisturbed for a few hours. Brownian motion is essential for the entropy driven self-assembly process we plan to use to form a photonic crystal and therefore this sample is unsuitable for that purpose. Also, even if it were possible to form a 3-dimensional crystal with these SPs, the crystal would not be photonic because a photonic crystal must have periodicity on the same scale as wavelengths of light, so these SPs are about two orders of magnitude too big to form such a crystal. Although the low polydispersity of these SPs is promising, their size makes them unsuitable to form a photonic crystal. Despite that, spherical SPs such as these have been shown to emit from whispering gallery modes[29] which means they have the potential to exhibit lasing because the spherical shape allows them to act as optical cavities.

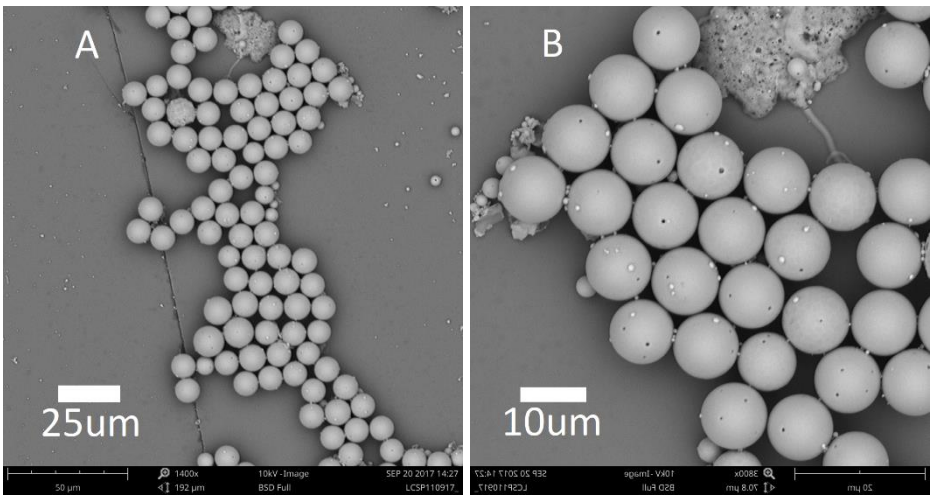

Figure 15. SEM images of SPs (A,B) formed using a dispersed phase with initial concentration of 10 mg/ml

Dispersed Phase Concentration

When using the emulsion-based method for the formation of SPs, there are two ways of reducing the size of the SPs formed. To create smaller SPs we need to reduce the number of NCs in each droplet, so we can (1) decrease the initial size of the droplets or (2) decrease the concentration of NCs in the dispersed phase. The extent to which we could decrease droplet size was limited by the microfluidics device we used so we chose to investigate using a lower concentration dispersed phase. The dispersed phase concentration was reduced to 1 mg/ml and conditions for the evaporation remained the same as our initial SP synthesis. The resulting SPs were imaged using SEM (Figure 16). From analysis of the images we measured a polydispersity of 4.2% and mean diameter of 4.4 µm. The decrease in size, compared to the sample made using a 10 mg/ml dispersed phase solution (Fig.15), confirms that it is possible to control SP size by changing the initial concentration of the dispersed phase. Although size is reduced, and low polydispersity is maintained, the SPs seem to show slight deformation from the perfectly spherical shape and their surfaces are covered in cracks and craters. These defects in the surface suggest that NCs inside the emulsion droplets are not behaving as hard spheres, as is required for this self-assembly process. The difference is clear when compared to the SPs produced from a 10 mg/ml dispersed phase solution (Fig.15)

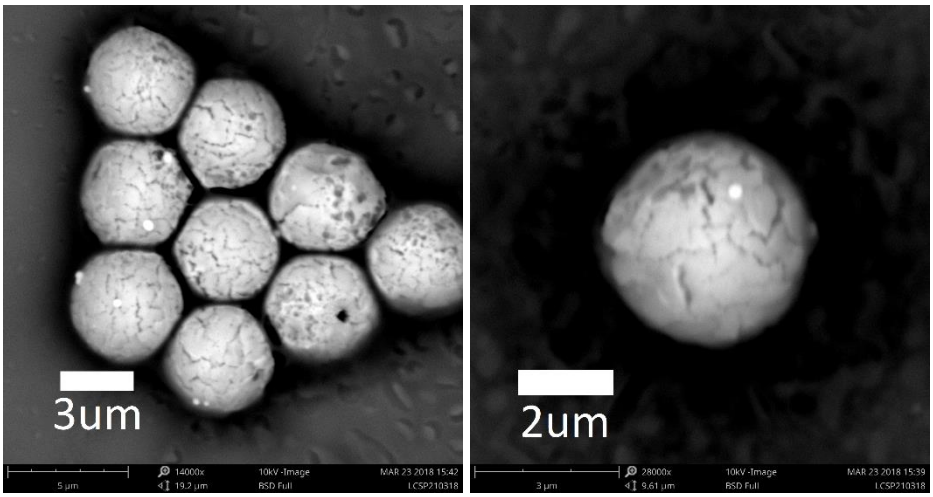

Figure 16. SEM images of SPs produced form 1 mg/ml solution of CdSe/CdS nanocrystals

A possible explanation for this difference may be that NC solvent is evaporating at a higher rate for the SPs formed using the lower concentration dispersed phase solution. For the evaporation process to proceed, the dispersed phase solvent molecules must transfer into the continuous phase and then evaporate to the surrounding atmosphere. When the vial is left open to atmosphere, the limiting step to this process is the transfer of solvent molecules to the continuous phase, so that rate at which this occurs is important to consider. For the entropy driven formation of SPs based on the hard sphere model, the NCs behaving as hard spheres will begin to crystallize when they reach a volume fraction of 0.494.[38] For the process carried out with the lower concentration disperse phase, the evaporating droplets are smaller in size when this volume fraction is reached. Our calculations show that, for droplets with an initial diameter of 55 µm, the 10 mg/ml dispersed phase solution will reach a volume fraction of 0.494 when the droplet diameter shrinks to 22 µm but for the 1mg/ml solution the droplets must shrink to 6 µm. This is significant because it is likely that the rate that droplets shrink increases as their size decreases, due to the Laplace pressure. The Laplace pressure describes the pressure difference inside a droplet compared to its surroundings (eq 10). The pressure increases inside the droplet as it decreases in size, which may increase the rate at which solvent molecules transfer from the droplet to the continuous phase, increasing the rate that droplet size

decreases.[63–65] This means that for lower concentration dispersed phase solutions, droplet size may be decreasing at a higher rate when crystallization begins to occur, which may prevent the system from reaching its lowest energy crystalline state.

$$p_{in} = p_{out} + 2\frac{\gamma}{r} \qquad (10)$$

Evaporation Time

To confirm whether this increase in evaporation rate with decreasing droplet size was the reason for defects seen in SPs in Fig.16, we investigated extending the evaporation time. The vial in which evaporation took place was sealed, leading to saturation of the atmosphere inside the vial with solvent vapour. Saturation of the atmosphere in the vial slows the rate of evaporation of solvent molecules from the continuous phase to atmosphere. This in turn, leads to saturation of the continuous phase with solvent molecules, which slows the rate that solvent molecules transfer from the droplets to the continuous phase. This pile up effect leads to a slower reduction of droplet size. We varied the evaporation time by changing the size of the vial, and therefore the volume of atmosphere above the emulsion (Fig.17). Using a dispersed phase with a concentration of 1 mg/ml, evaporation time was increased to 21hrs (Fig.17A,B) and 45hrs(Fig.17C,D).

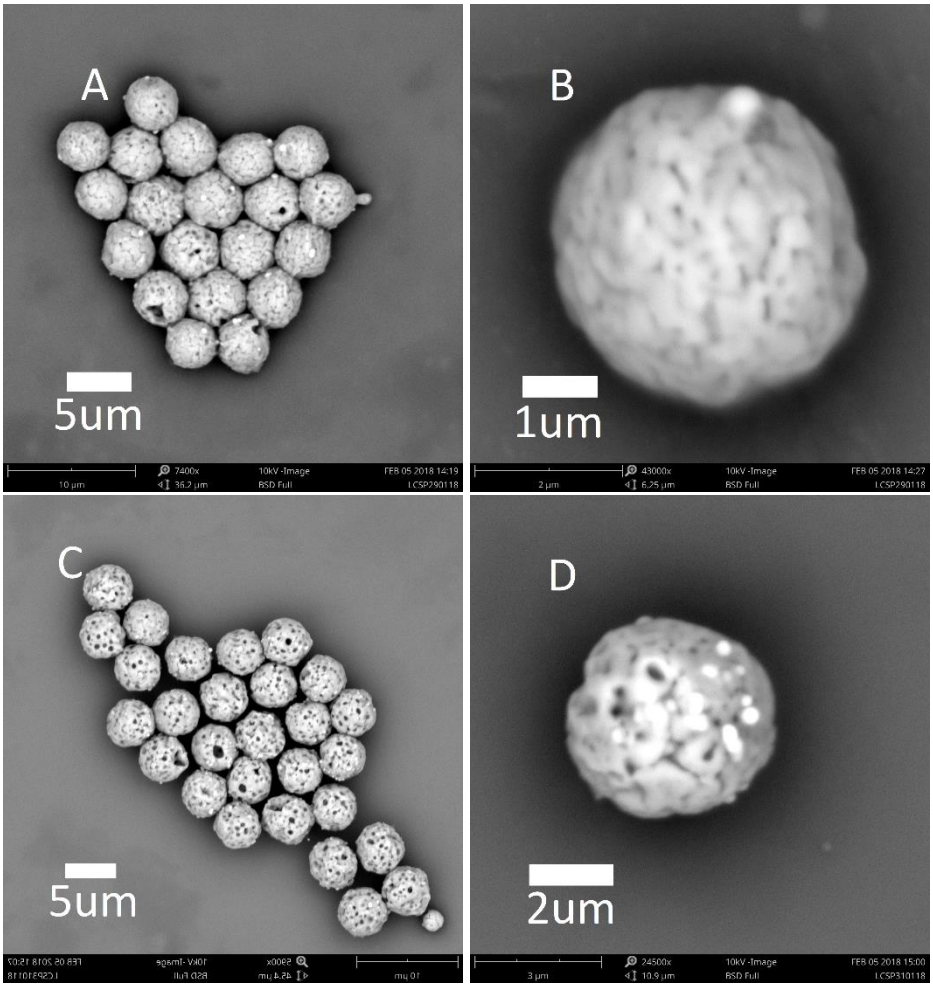

Figure 17. SEM images of SPs formed with evaporation time of 21 hours (A,B) and 46 hours (C,D)

The resulting SPs were imaged using SEM and from the images, we calculated the polydispersity an average size of both samples. The sample formed after evaporation for 21hrs had mean diameter of 4.33 µm and polydispersity of 4.6%. the sample formed after evaporation for 45hrs

had a mean diameter of 4.76 µm and a polydispersity of 4.2%. The difference in average size is due to a slight difference in the initial droplet size. The larger sample was made from droplets with an initial diameter of 64 µm compared to 62 µm for the smaller sample. Polydispersity is unaffected by the change in evaporation time. The increased evaporation time also seems to have no effect on the quality of the SP surface, with cracks and craters still covering the surfaces of SPs, and no clear difference between the two samples. This result suggests that the evaporation rate is not the reason for the irregular SP surfaces we are seeing. Another possible explanation for this is, the NCs in solution are not behaving as hard spheres due to interparticle interactions causing them to aggregate before the point of crystallization and preventing them from reorganising into a crystalline assembly as higher volume fractions are reached.

Increased Temperature

Another way to influence SP formation is by controlling the temperature of the system in which self-assembly is taking place. We want to achieve entropically-driven self-assembly of colloidal hard spheres. To achieve this we need the system to be under thermodynamic control and we also need entropy to dominate over any enthalpic interactions.[34–36,66] In theory, raising the temperature increases the thermal energy of the system, allowing entropy to dominate and overcome any enthalpic interactions such as attractive inter-particle forces.[43,66,67] For this reason we investigated raising the temperature by using a thermofoil to heat the vial containing the emulsion. The exact temperature inside the vial was not known but the thermofoil was shown to heat the continuous phase solution to a temperature of 40°C under normal atmospheric conditions so we assume the temperature during SP formation was around 40°C. The vial was sealed during evaporation, to prevent the increase in temperature speeding up the evaporation. The initial dispersed phase concentration was 1 mg/ml and the evaporation took between 21-46hrs. The resulting SPs were imaged using SEM and the images show very deformed SPs with very irregular shapes, which made it impossible to measuring the average size and polydispersity for this sample.

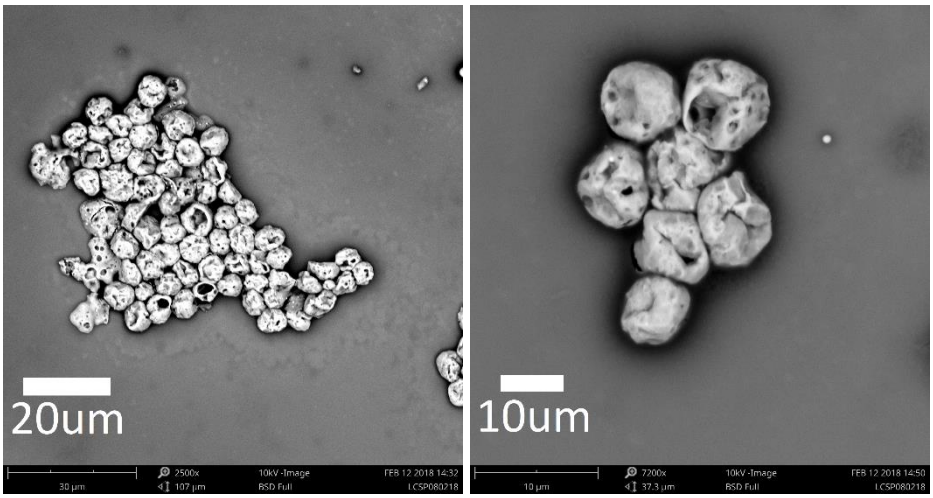

Figure 18. SEM images of SPs formed at higher temperature

The poor quality of the SPs formed could be explained by fluid flows and solvent fluctuations that occur within the droplet during late-stage drying, and are exacerbated by the increase in temperature, preventing the system reaching equilibrium conditions.[68,69] Another possible explanation is that the increase in temperature may contribute to an increase in droplet deformation. Droplet deformation is affected by the size of the droplet and the interfacial tension between the two phases. In the paper by Tolstogusov et al[70] the droplet axial ratio, the measure of deformation used,

increases with droplet volume and decreases with increasing interfacial tension. Increasing the temperature of a two-phase system, such as an emulsion, lowers the interfacial tension between the phases. Raising the temperature may have increased the extent to which the droplets were deformed by stirring, during the evaporation step of the process and led to the deformed assemblies we observed (Fig.18).

Solvent Effects

As another way to try and improve the quality of the SPs were making, we investigated the influence of NC solvent on the self-assembly process. There are two main reasons why changing the NC solvent used could have an effect on SP formation. The first reason is that the interaction of solvent molecules with the organic ligands stabilising NCs surfaces can have a big effect on the dispersibility of the NCs in the solvent.[71] Increasing the dispersibility of NCs, allows them to behave more as hard spheres, which is preferable for our chose self-assembly method. The second reason is that the interfacial tension between the solvent and the aqueous continuous phase can have a big effect on self-assembly, so the interfacial tension between solvent and water is a factor that needs to be considered. A higher interfacial tension could cause NCs to absorb to the droplet surface because the presence of NCs at the surface reduces the area of the solvent-water interface, thereby decreasing the total free energy of the system.[44] The change in energy of the system due to the absorption of an individual nanocrystal, with radius r, to the interface is given by equation 11.[42]

$$\Delta E = -\frac{\pi r^2}{\gamma_{ow}}[\gamma_{ow} - (\gamma_{pw} - \gamma_{po})]^2 \qquad (11)$$

It is calculated using the interfacial tension values for the oil/water (γ_{ow}), particle/water (γ_{pw}) and particle/oil (γ_{po}) interfaces. The values for the oil/water interfacial tension were retrieved from literature. The values used for particle/water and particle/oil interfacial tensions were reported in the paper by Kutusov et al[42] for CdSe nanocrystals in a toluene/water system. If this change in energy is greater in magnitude than the thermal energy k_bT, then particles NCs will absorb to and be held at the interface.[45] We calculated this energy change for different solvents to determine which would be interesting to use (Table 5).

Solvent	Interfacial tension with water-SDS solution @293K (mN/m)	ΔE @293K (kT)	Boiling point (K)	Solubility in water (mg/L)
Cyclohexane	40*	-85	353	55
Hexane	42.9[47]	-110	342	9.5
Heptane	43.1*	-113	371	3
Toluene	29.5[46]	-12	384	520

Table 5. Properties of different dispersed phase solvents. Values marked with * were estimated based on other literature values.

Our first thought was to try using toluene as the dispersed phase solvent but the high solubility of toluene in water meant that evaporation of toluene droplets occurred very quickly, which is not conducive to the formation of SPs. We chose instead to use Heptane as the NC solvent. The dispersed phase for this sample was composed of a 1.5 mg/ml solution FeO/$CoFe_2O_4$ core/shell NCs dispersed in heptane. The resulting SPs were imaged using SEM (Fig.19). The change in solvent clearly had a negative effect on SP formation, with very misshapen, irregular structures formed. Average size and polydispersity were not measured for this sample because of the irregular shapes of the SPs. Figure

19 shows an SP sample formed from the same NCs but using cyclohexane as the solvent. Comparing these two samples confirms that the choice of solvent can have a big impact on SP formation.

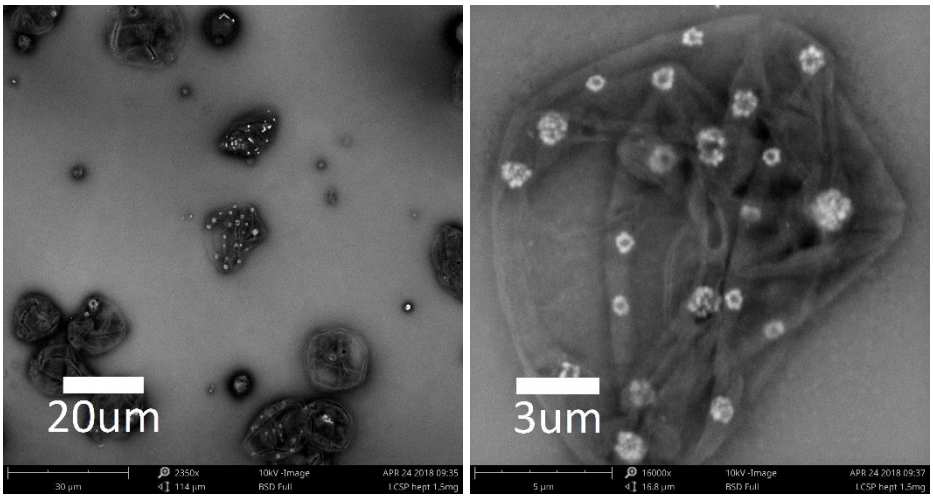

Figure 19. SEM images of SPs produced using heptane as the dispersed phase solvent.

Raising the interfacial tension of the system, as we did by changing the solvent from cyclohexane to heptane, may have caused particles to absorb to the interface to minimize its surface area and lower the energy of the system overall.[44] The higher the interfacial tension the stronger particles will be absorbed to the interface.[42] The absorption of NCs to the interface paired with the high flux of particles to the interface due to the shrinking of the droplet[72], could lead to a disproportionately high concentration at the interface which in turn could lead to nucleation and aggregation of NCs at the interface. Also, capillary forces may be acting on NCs absorbed to the surface causing them to aggregate. It is possible that a thin shell of NCs is formed at the droplet surface, which then is forced to collapse on itself as the droplet shrinks further.

Interparticle forces

Next, we chose to investigate the influence of interactions between NCs on SP formation. For all of the previous samples we have tried to minimize any interaction between particles, to allow the NCs involved to behave as hard spheres. In our case it is counter intuitive to use particles with greater interactions because such particles can only behave less like hard spheres but, interactions between particles have been shown to benefit self-assembly processes under certain conditions[73,74] and metallic NCs have been used to successfully form SPs before.[34,75] For this reason, we investigated the use of metallic NCs for SP formation. We used metallic NCs to form SPs because they are expected to have stronger interactions compared to semiconductor NCs. Metallic NCs are more easily polarizable than their semiconductor counterparts, leading to stronger interactions between particles due to electrostatic forces.[43] The metallic NCs used here also exhibit magnetic interactions.[51] For the dispersed phase, we used a 1.62 mg/ml solution of $FeO/CoFe_2O_4$ core/shell NCs dispersed in cyclohexane. The resulting SPs were imaged using SEM (Fig.20). From analysis of the images we measured a mean particle diameter of 5.67 µm and polydispersity of 3.7%. The polydispersity is exceptionally low, and this is demonstrated by the ordered hexagonal packing of SPs when deposited on Si wafer for analysis. The SPs have well defined spherical shape, but the quality of SP surface varies. Around half the particles have smooth surfaces, as we saw with our initial synthesis that used a 10 mg/ml dispersed phase solution. The other half of SPs appear to have surfaces covered in holes. It is difficult to concluded anything about the influence of interactions between NCs in SP formation from these results.

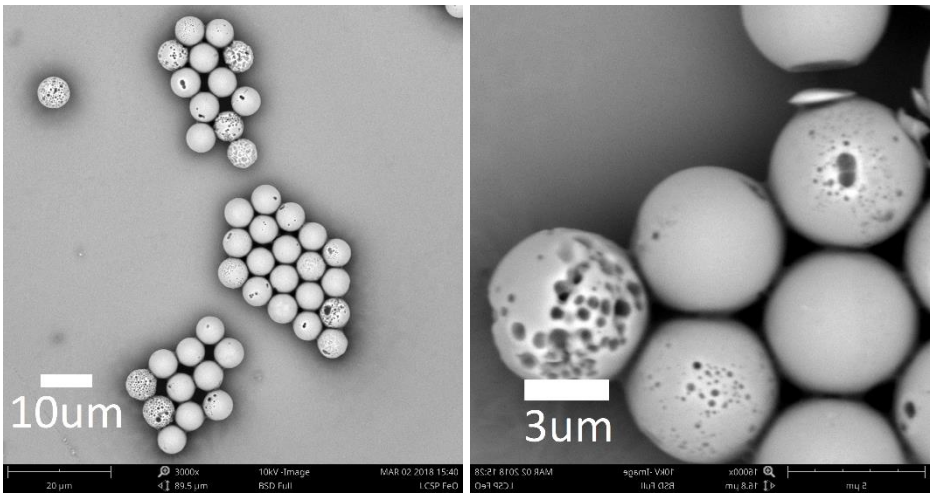

Figure 20. SEM images of SPs formed using metallic nanocrystals

Supraparticles: Sonication as Emulsification Technique

We also produced SPs using sonication as the emulsification method. Sonication is a quick and easy way of forming an emulsion with droplet sizes on the micrometer and nanometer scale. The disadvantage of sonication as an emulsification technique is a lack of control over the size and polydispersity of the droplets formed. Previous work[59] using sonication as an emulsification technique to form SPs has shown high polydispersity of the SPs formed. Such samples are not suitable for the formation of a photonic crystal through self-assembly so our motivation for using this technique was to investigate the effect of initial dispersed phase concentration on SP formation. It has already been shown in our previous results that decreasing the initial dispersed phase concentration from 10 mg/ml – 1mg/ml is detrimental to quality of the SPs formed. By using sonication, we can form SPs of a similar size to the ones formed from microfluidics, using a dispersed phase with a much higher initial concentration.

Both low and high-power sonication method were used as outlined in the methods section. The distinction between the low and high power is based on the frequencies that can be used. High-power uses higher frequencies so can produce smaller droplets. We used both CdSe/CdS QDs and $FeO/CoFe_2O_4$ NCs, with initial dispersed phase concentrations of 16 mg/ml and 37.6 mg/ml respectively. The SPs formed were imaged by either TEM or SEM, depending on the size of the SPs produced. SPs produced from low power sonication can be clearly observed using SEM but those produced using high power are smaller and therefore more difficult to see clearly with SEM. For this reason, TEM was a more appropriate technique for the analysis of the SPs produced using high power sonication. From analysis of the TEM and SEM images we measured average size and polydispersity for each sample, but we were unable to obtain images of the QD sample made with high power sonication due to an error in preparing the sample (table 5).

Method	**NCs**	**Mean Diameter (nm)**	**Polydispersity (%)**
High power	$FeO/CoFe_2O_4$	46	37
Low power	$FeO/CoFe_2O_4$	468	32
Low power	CdSe/CdS	720	49

Table 5. Results of analysis of SEM images of samples formed using sonication as an emulsification technique

TEM was used to image the SP sample formed from $FeO/CoFe_2O_4$ NCs using high power sonication (Fig.21A,B). With a mean diameter of 46nm, the SPs in this sample are far smaller than those in samples produced using microfluidics so it is hard to make any comparisons. The images show that most SPs are at least partially crystalline, which supports the results we obtained from TEM images of SPs formed using the shear cell and confirms that it is possible to form crystalline SPs using an emulsion-based method. SEM was used to image the SPs formed from CdSe/CdS QDs (Fig.21C,D) and $FeO/CoFe_2O_4$ NCs (Fig.21E,F) using low power sonication. These samples are closer in size to those formed with microfluidics. The SPs formed have well defined spherical shape and no surface defects are visible. This confirms that the initial concentration of the dispersed phase has a significant effect on SP formation and a decrease in concentration is responsible for the appearance of defects and irregularities on SP surfaces. The reasons for this are not clear but it is probably a combination of multiple factors. The disadvantage of using sonication as an emulsification technique is evident from the high polydispersity measured for all the samples. The high polydispersity of these samples renders them unsuitable to form a photonic crystal through hierarchical self-assembly.

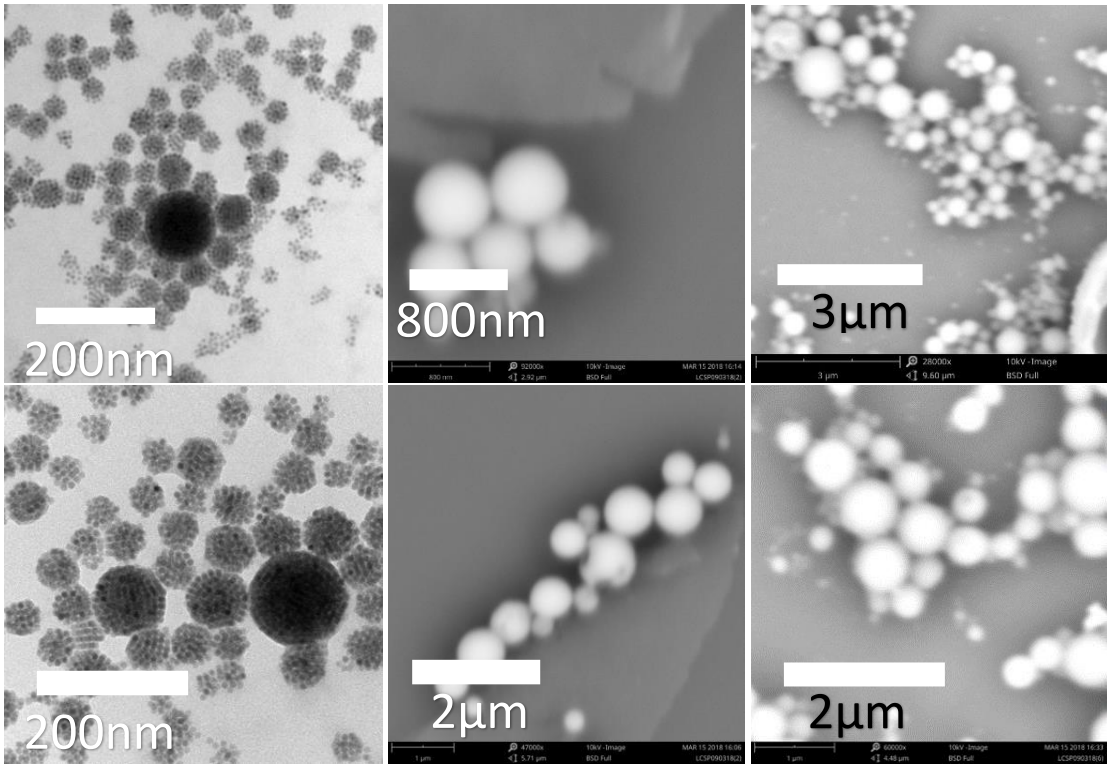

Figure 21 TEM images of SPs formed from $FeO/CoFe_2O_4$ NCs using high power sonication(A,B). SEM images of SPS formed form $FeO/CoFe_2O_4$ NCs (C,D) and from CdSe/CdS QDs (E,F) using low power sonication.

A possible explanation for the effect of initial dispersed phase concentration is that a lower concentration dispersed phase leads to a concentration gradient within droplets and this has a detrimental effect on SP formation. Due to adsorption of NCs to the droplet surface, in a dilute solution a majority of NCs are likely to be at the interface. As the droplet shrinks, the higher concentration at the droplet surface may cause NCs to aggregate and capillary forces could cause particles adsorbed to the surface to attach, forming a shell which collapses in on itself as the droplet shrinks further. For a more concentrated solution, after the interface becomes saturated with NCs, there are still a high concentration of NCs in the bulk of the droplet This Decreases the chance of a concentration gradient existing between the surface and the bulk of the droplet and gives a better chance of forming a densely packed or crystalline SP (Fig.22)

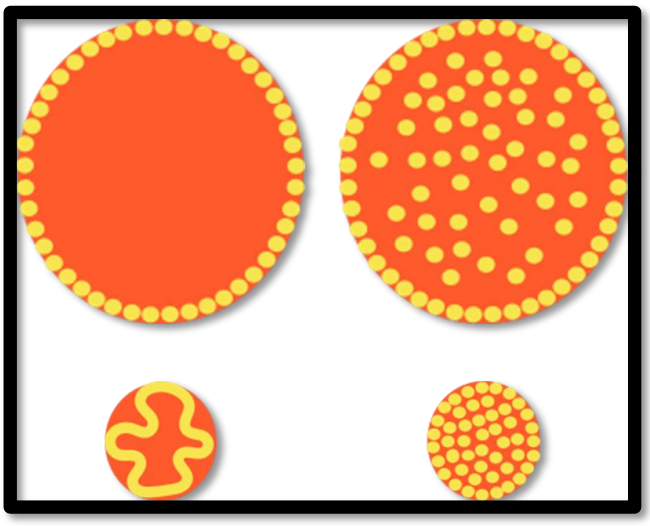

Figure 22. Schematic representation of the difference between a droplet formed low initial dispersed phase concentration compared to a droplet formed with high initial dispersed phase concentration

Conclusions and Outlook

The goal of this research project was to create a structure that couples the photoluminescent properties of QDs with the photonic properties of a photonic crystal. We hoped to realise this goal through hierarchical self-assembly, using QDs to form colloidal SPs, which in turn could be used to form a photonic crystal. To achieve this goal, we needed to produce a monodisperse sample of crystalline SPs. We hoped to achieve this through the 3-D confinement of NCs using an emulsion-based method. This method requires an entropy driven process in which interparticle attractions and attraction of particles to the interface of the two-phase system are minimized, allowing the NCs to behave as hard spheres.[34] Our results show that, for our emulsion based method, there are challenges to creating a system in which NCs behave as hard spheres, especially for SP samples formed from a dispersed phase with a lower initial concentration. With this section we aim to explain why this was the case based on the results obtained during the project and other results from literature. Finally, we offer our ideas about how best to proceed with this research if the final goal is to be achieved.

Emulsification Methods

The polydispersity of SPs formed using an emulsion-based method is dependent on the polydispersity of the emulsion droplets. To form monodisperse SPs we need an emulsification method that produces monodisperse droplets. We used three different emulsification methods during this project. Microfluidics, sonication and mechanical mixing with a Taylor-Coutte shear cell.

The use of microfluidics as emulsification method is time consuming and the droplet sizes achievable are limited by the microfluidics device used. The advantages include fine control of droplet size within a certain range and monodisperse droplets. All SP samples formed using microfluidics had a polydispersity lower than 5% which is a very promising outcome. The disadvantage of using microfluidics is that the size of the droplets produced is limited by the microfluidics device being used. Our microfluidics chip could only reliable produce monodisperse droplets in the size range of 45-85µm, so we were forced to explore other options for reducing the size of the SPs produced.

We investigated the use of mechanical mixing and sonication as emulsification methods. These methods offer the advantage of making smaller droplets relative to our microfluidics setup, making it easier to form SPs on the scale we need to create a photonic crystal. The reason we didn't pursue the use of these methods any further was the high polydispersity (≥30%) of the samples produced. Obtaining a monodisperse SP sample using these methods would have required processing of samples after the evaporation step to separate the SPs by size and it is unclear whether this would work.

Microfluidics is the method with the greatest potential to form SP samples useful for creating a photonic crystal through hierarchical self-assembly. The primary reason being the monodispersity of droplets formed, but the ability to adjust droplet size within a certain range would also be very useful as it would allow fine tuning of the SP size. This would allow fine tuning of the photonic band gap of the photonic crystal formed using these SPs. The goal of this research project was to create a structure that couples the photoluminescent properties of QDs with the photonic properties of a photonic crystal by creating an overlap between the emission spectrum of the QDs and the photonic band gap of the photonic crystal. Fine control over the position of the photonic band gap would be vital for achieving this goal. More sophisticated microfluidics devices exist that can produce monodisperse droplets on smaller scale and using one of these to form SPs is the next logical step to achieving the goal of this project.

Supraparticle Formation

From our initial experiment forming SPs using droplets made by microfluidics, the low SP polydispersity of 4% was a promising outcome but the SPs were too large to be colloidally stable, rendering them unsuitable for hierarchical self-assembly. The droplet size could not be reduced further because of the limitations of the microfluidics device, so we tried lowering the concentration of NCs in the dispersed phase to decrease the size of the SPs formed. This negatively affected SP formation, causing defects such as cracks and craters to appear on SP surfaces. From this point on, our experiment focused on trying to optimize SP formation by investigating the effects of changing various parameters

Evaporation Time

We investigated the effects of lengthening the droplet evaporation time by saturating the atmosphere above the emulsion with solvent. In theory a longer evaporation time should help to ensure the system experiences equilibrium conditions. We formed samples with evaporation times of 12, 21 and 45 hrs. There was no apparent difference between the samples and all of them possessed the same irregular surfaces. From this we can conclude that the irregular SPs surfaces are not a result of the evaporation time and are likely caused by a different factor.

Temperature

Next we investigated raising the temperature to increases the thermal energy of the system, allowing entropy to dominate and overcome any enthalpic interactions such as attractive inter-particle forces.[43,66,67] The temperature during SP formation was raised from room temperature to 40°C. This was detrimental to SP formation, the SPs formed were very deformed and irregularly shaped. This can be explained by the present of fluid flows and solvent fluctuations that occur within the droplet during late-stage drying, and are exacerbated by the increase in temperature, preventing the system reaching equilibrium conditions.[68,69] Although in theory, raising the temperature of the colloidal system should be favourable for entropy driven self-assembly, it is not an effective approach for improving the conditions for SP formation in our case because of the way it affects droplet drying.

Interfacial Tension

The interfacial tension between the dispersed phase and the continuous phase is an important factor to consider in the SP formation process. The interfacial tension depends on the solvent used for the dispersed phase but is also affected by other factors such as temperature and the presence of a surfactant.[47] From our results it seems that both increasing and decreasing interfacial tension can have negative effects on SP formation, and more detailed study is required to determine what is happening. Our experiment using heptane as the NC solvent, instead of cyclohexane, showed that the solvent used can have a hugely significant effect on SP formation and this may be caused by the change in interfacial tension between phases when the solvent is changed. Raising the interfacial tension of the system, as we did by changing the solvent, can cause particles to absorb to the interface to minimize its surface area and lower the energy of the system overall.[44] The higher the interfacial tension the stronger particles will be absorbed to the interface.[42] The absorption of NCs to the interface paired with the high flux of particles to the interface due to the shrinking of the droplet[72], could lead to a disproportionately high concentration at the interface which in turn could lead to nucleation and aggregation of NCs at the interface. If nucleation and aggregation occur at different points on the interface, NCs are no longer free to reorganize into a densely packed crystal structure as the droplet shrinks further, leading to the SP surfaces with cracks and craters that we observed in many of our experiments. We can't determine the exact role of the interfacial tension in the SP formation process from these results because too many variables are changed and there are several different factors that may have an influence. More detailed studies into the use of different solvents and the influence of temperature are needed to determine how these factors are affecting SP formation.

Initial Concentration of Dispersed Phase

Another factor that clearly influenced SP formation was the initial NC concentration in the dispersed phase. Sample formed from a higher dispersed phase had smooth surfaces and were spherical. When initial concentration of dispersed phase was reduced defects appeared in the surfaces of SPs. A possible explanation is that at low concentrations a majority of NCs are absorbed to the droplet surface and there is a difference in concentration between the droplet surface and the bulk of the droplet. This may causes crystallization and aggregation of NCs at different points of the droplet surface.[72] As the droplet shrinks further, the strong interactions between clustered NCs hinders their reorganization into one densely packed assembly. If a higher concentration dispersed phase is used, the concentration difference between the bulk and surface of the droplet will be lessened, increasing the chance that crystallization will occur at the surface and in the bulk at the same time to form one crystalline assembly.

Outlook

Although we failed to achieve the goal of this research, the results obtained, and similar examples from literature, lead me to believe that it is possible to achieve this goal. It would be interesting to investigate the effect of using different stabilizing ligands at the NC surface. The paper by Yang et al[71] shows the use of n-alkanoates as stabilizing ligands greatly increases NC solubility by 10^2-10^6 times. They showed that solutions with concentrations as high as 1000 mg/ml could be made. The use of these ligands to stabilize NCs used for SP formation would help ensure they behave as hard spheres, as is required for the entropically driven formation of SPs by 3-d confinement.

There is scope for more detailed study into the effect of NC solvent used for the dispersed phase. Our results showed that changing solvent had a dramatic effect on the SPs formed, but a more detailed study is required to determine the exact reason for this. For example, an experiment investigating

emulsion-based SP formation in a variety of solvents that have varying interfacial tensions with the continuous phase. The same goes for the temperature that the process is carried out at. In our results an increase in temperature had a big effect on the SPs formed but the reason for this could not be determined exactly. We investigated raising the temperature and found this to have a detrimental effect on SP formation but it would be interesting to see how a decrease in temperature would affect SP formation.

The use of microfluidics was successful for creating monodisperse SPs but the limitations of the device we used meant droplet size was too large to form SPs on the scale we needed to create a photonic crystal. The use of a more sophisticated microfluidics device that can produce smaller droplets, and thereby allowing the use of a relatively high concentration of NCs in the dispersed phase, would greatly improve the chances of forming monodisperse SPs on the desired scale.

References

1. Buzea, C., Pacheco, I. I. & Robbie, K. Nanomaterials and nanoparticles: Sources and toxicity. *Biointerphases* **2,** MR17-MR71 (2007).
2. Barbaro, P. & Liguori, F. *Heterogenized Homogeneous Catalysts for Fine Chemicals Production: Materials and Processes*. (Springer Netherlands, 2010).
3. Roduner, E. Size matters: why nanomaterials are different. *Chem. Soc. Rev.* **35,** 583 (2006).
4. Alivisatos, A. P. Perspectives on the physical chemistry of semiconductor nanocrystals. *J. Phys. Chem.* **100,** 13226–13239 (1996).
5. De Mello Donegá, C. *Nanoparticles: Workhorses of nanoscience*. *Nanoparticles: Workhorses of Nanoscience* **9783662448,** (2014).
6. Kalesaki, E. *et al.* Dirac Cones , Topological Edge States , and Nontrivial Flat Bands in Two-Dimensional Semiconductors with a Honeycomb Nanogeometry. **011010,** 1–12 (2014).
7. Boneschanscher, M. P. *et al.* Long-range orientation and atomic attachment of nanocrystals in 2D honeycomb superlattices. **344,** 1377–1381 (2014).
8. Ito, T. & Okazaki, S. Pushing the limits of lithography. **406,** 1027–1031 (2000).
9. Tadepalli, S., Slocik, J. M., Gupta, M. K., Naik, R. R. & Singamaneni, S. Bio-Optics and Bio-Inspired Optical Materials. *Chem. Rev.* acs.chemrev.7b00153 (2017). doi:10.1021/acs.chemrev.7b00153
10. Zi, J. *et al.* Coloration strategies in peacock feathers. **2003,** (2003).
11. Guo, M. *et al.* Broadband and omnidirectional light harvesting enhancement in photovoltaic devices with aperiodic TiO2nanotube photonic crystal. *J. Power Sources* **345,** 12–20 (2017).
12. Knight, J. Photonic crystal fibres. *Nature* **424,** 847–851 (2003).
13. Yanik, M. F., Fan, S., Soljačić, M. & Joannopoulos, J. D. All-optical transistor action with bistable switching in a photonic crystal cross-waveguide geometry. *Opt. Lett.* **28,** 2506 (2003).
14. Atkins, P. *et al. Shriver & Atkins' Inorganic Chemistry, Fifth Edition*.
15. Joannopoulos, J. J. D., Johnson, S., Winn, J. N. J. & Meade, R. R. D. *Photonic crystals: molding*

the flow of light. *Time* (2008). doi:10.1063/1.1586781

16. Ge, J., Hu, Y., Biasini, M., Beyermann, W. P. & Yin, Y. Superparamagnetic magnetite colloidal nanocrystal clusters. *Angew. Chemie - Int. Ed.* **46,** 4342–4345 (2007).

17. Yi, D. K. *et al.* Silica-Coated Nanocomposites of Magnetic Nanoparticles and Quantum Dots. 4990–4991 (2005). doi:10.1021/ja0428863

18. Zhuang, J., Wu, H., Yang, Y. & Cao, Y. C. Controlling colloidal superparticle growth through solvophobic interactions. *Angew. Chemie - Int. Ed.* **47,** 2208–2212 (2008).

19. Bai, F. *et al.* A versatile bottom-up assembly approach to colloidal spheres from nanocrystals. *Angew. Chemie - Int. Ed.* **46,** 6650–6653 (2007).

20. Montanarella, F. *et al.* Composite Supraparticles with Tunable Light Emission. *ACS Nano* **11,** 9136–9142 (2017).

21. Li, X. H., Li, J. X., Li, G. D., Liu, D. P. & Chen, J. S. Controlled synthesis, growth mechanism, and properties of monodisperse CdS colloidal spheres. *Chem. - A Eur. J.* **13,** 8754–8761 (2007).

22. Chen, O. *et al.* Magneto-fluorescent core-shell supernanoparticles. *Nat. Commun.* **5,** 5093 (2014).

23. Mekis, I., Talapin, D. V., Kornowski, A., Haase, M. & Weller, H. One-Pot Synthesis of Highly Luminescent CdSe/CdS Core−Shell Nanocrystals via Organometallic and “Greener” Chemical Approaches †. *J. Phys. Chem. B* **107,** 7454–7462 (2003).

24. Cao, H. *et al.* Design and Synthesis of Antiblinking and Antibleaching Quantum Dots in Multiple Colors via Wave Function Confinement. *J. Am. Chem. Soc.* jacs.6b10102 (2016). doi:10.1021/jacs.6b10102

25. Carbone, L. & Cozzoli, P. D. Colloidal heterostructured nanocrystals: Synthesis and growth mechanisms. *Nano Today* **5,** 449–493 (2010).

26. Omogo, B., Gao, F., Bajwa, P., Kaneko, M. & Heyes, C. D. Reducing Blinking in Small Core-Multishell Quantum Dots by Carefully Balancing Confinement Potential and Induced Lattice Strain: The ‘goldilocks’ Effect. *ACS Nano* **10,** 4072–4082 (2016).

27. Chen, O. *et al.* Compact high-quality CdSe-CdS core-shell nanocrystals with narrow emission linewidths and suppressed blinking. *Nat. Mater.* **12,** 445–51 (2013).

28. Li, J. J. *et al.* Large-scale synthesis of nearly monodisperse CdSe/CdS core/shell nanocrystals using air-stable reagents via successive ion layer adsorption and reaction. *J. Am. Chem. Soc.* **125,** 12567–12575 (2003).

29. Vanmaekelbergh, D. *et al.* Shape-dependent multiexciton emission and whispering gallery modes in supraparticles of CdSe/multishell quantum dots. *ACS Nano* **9,** 3942–3950 (2015).

30. Reiss, P., Protière, M. & Li, L. Core/shell semiconductor nanocrystals. *Small* **5,** 154–168 (2009).

31. Lamer, V. K. & Dinegar, R. H. Theory, Production and Mechanism of Formation of Monodispersed Hydrosols. *J. Am. Chem. Soc.* **72,** 4847–4854 (1950).

32. Sugimoto, T. Preparation of monodispersed colloidal particles. *Adv. Colloid Interface Sci.* **28,** 65–108 (1987).

33. Yu, W. W., Qu, L., Guo, W. & Peng, X. Experimental determination of the extinction coefficient of CdTe, CdSe, and CdS nanocrystals. *Chem. Mater.* **15,** 2854–2860 (2003).

34. De Nijs, B. *et al.* Entropy-driven formation of large icosahedral colloidal clusters by spherical confinement. *Nat. Mater.* **14,** 56–60 (2015).

35. Eldridge, M. D., Madden, P. A. & Frenkel, D. Entropy-driven formation of a superlattice in a hard-sphere binary mixture. *Nature* **365,** 35–37 (1993).

36. Evers, W. H. *et al.* Entropy-driven formation of binary semiconductor-nanocrystal superlattices. *Nano Lett.* **10,** 4235–4241 (2010).

37. Vanmaekelbergh, D. Self-assembly of colloidal nanocrystals as route to novel classes of nanostructured materials. *Nano Today* **6,** 419–437 (2011).

38. Hoover, W. G. & Ree, F. H. Melting Transition and Communal Entropy for Hard Spheres. *J. Chem. Phys.* **49,** 3609–3617 (1968).

39. P. G. Bolhuis, D. F. Entropy difference between crystal phases. *Nature* **388,** 236–236 (1997).

40. Rosenbluth, M. N. & Rosenbluth, A. W. Further Results on Monte Carlo Equations of State. *J. Chem. Phys.* **22,** 881–884 (1954).

41. Löwen, H. Melting, freezing and colloidal suspensions. *Phys. Rep.* **237,** 249–324 (1994).

42. Kutuzov, S. *et al.* On the kinetics of nanoparticle self-assembly at liquid/liquid interfaces. *Phys. Chem. Chem. Phys.* **9,** 6351 (2007).

43. Bishop, K. J. M., Wilmer, C. E., Soh, S. & Grzybowski, B. A. Nanoscale forces and their uses in self-assembly. *Small* **5,** 1600–1630 (2009).

44. Manoharan, V. N. Colloidal spheres confined by liquid droplets: Geometry, physics, and physical chemistry. *Solid State Commun.* **139,** 557–561 (2006).

45. Manoharan, V. N. Dense Packing and Symmetry in Small Clusters of Microspheres. *Science (80-.).* **301,** 483–487 (2003).

46. Saien, J. & Akbari, S. Interfacial tension of toluene + water + sodium dodecyl sulfate from (20 to 50) °C and pH between 4 and 9. *J. Chem. Eng. Data* **51,** 1832–1835 (2006).

47. Saien, J., Rezvani Pour, A. & Asadabadi, S. Interfacial tension of the n-hexane-water system under the influence of magnetite nanoparticles and sodium dodecyl sulfate assembly at different temperatures. *J. Chem. Eng. Data* **59,** 1835–1842 (2014).

48. Rallison, J. M. THE DEFORMATION OF SMALL VISCOUS DROPS AND BUBBLES IN SHEAR FLOWS. *Annu. Rev. Fluid Mech.* 45–66 (1984). doi:0066-4189/84/0115-0045

49. Mason, T. G. & Bibette, J. Shear Rupturing of Droplets in Complex Fluids. *Langmuir* **13,** 4600–4613 (1997).

50. Maa, Y. F. & Hsu, C. C. Performance of sonication and microfluidization for liquid-liquid emulsification. *Pharm. Dev. Technol.* **4,** 233–240 (1999).

51. Bodnarchuk, M. I. *et al.* Exchange-coupled bimagnetic wüstite/metal ferrite core/shell nanocrystals: Size, shape, and compositional control. *Small* **5,** 2247–2252 (2009).

52. Haase, M. & Jasna, B. Tailoring of High-Order Multiple Emulsions by the Liquid–Liquid Phase Separation of Ternary Mixtures. *Angew. Chemie* **126,** 11987–11991

53. Mabille, C. *et al.* Rheological and shearing conditions for the preparation of monodisperse emulsions. *Langmuir* **16,** 422–429 (2000).

54. Peng, X., Wickham, J. & Alivisatos, A. P. Kinetics of II-VI and III-V colloidal semiconductor

nanocrystal growth: 'Focusing' of size distributions [15]. *J. Am. Chem. Soc.* **120,** 5343–5344 (1998).

55. Murray, C. B., Norris, D. & Bawendi, M. G. Synthesis and characterization of nearly monodisperse CdE (E= S, Se, Te) semiconductor nanocrystallites. *J. Am. Chem. Soc.* **115,** 8706–8715 (1993).

56. Cui, J. *et al.* Evolution of the Single-Nanocrystal Photoluminescence Linewidth with Size and Shell: Implications for Exciton-Phonon Coupling and the Optimization of Spectral Linewidths. *Nano Lett.* **16,** 289–296 (2016).

57. von Freymann, G., Kitaev, V., Lotsch, B. V. & Ozin, G. A. Bottom-up assembly of photonic crystals. *Chem. Soc. Rev.* **42,** 2528–2554 (2013).

58. Boles, M. A. & Talapin, D. V. Self-assembly of tetrahedral cdse nanocrystals: Effective 'patchiness' via anisotropic steric interaction. *J. Am. Chem. Soc.* (2014). doi:10.1021/ja501596z

59. de Nijs, B. *Towards Crystals of Crystals of Nanocrystals: a Self-Assembly Study*. (2014).

60. Zhang, X. Dynamics of drop formation in viscous flows. *Chem. Eng. Sci.* **54,** 1759–1774 (1999).

61. Baroud, C. N., Gallaire, F. & Emi Dangla, R. Dynamics of microfluidic droplets. doi:10.1039/c001191f

62. Cramer, C., Fischer, P. & Windhab, E. J. Drop formation in a co-flowing ambient fluid. *Chem. Eng. Sci.* **59,** 3045–3058 (2004).

63. Kayser, R. & Bennett, H. S. Evaporation of a liquid droplet. *J. Res. Natl. Bur. Stand. Sect. A Phys. Chem.* **81A,** 257 (1977).

64. Bao, J. Droplet Evaporation. (2007).

65. Teh, S.-Y., Lin, R., Hung, L.-H. & Lee, A. P. Droplet microfluidics. *Lab Chip* **8,** 198 (2008).

66. van Rijssel, J. *et al.* Enthalpy and entropy of nanoparticle association from temperature-dependent cryo-TEM. *Phys. Chem. Chem. Phys.* **13,** 12770 (2011).

67. Bodnarchuk, M. I., Kovalenko, M. V., Heiss, W. & Talapin, D. V. Energetic and entropic contributions to self-assembly of binary nanocrystal superlattices: Temperature as the structure-directing factor. *J. Am. Chem. Soc.* **132,** 11967–11977 (2010).

68. Deegan, R. D. *et al.* Capillary flow as the cause of ring stains from dried liquid drops. *Nature* **389,** 827–829 (1997).

69. Rabani, E., Reichman, D. R., Geissler, P. L. & Brus, L. E. Drying-mediated self-assembly of nanoparticles. *Nature* **426,** 271–274 (2003).

70. Tolstoguzov, V. B., Mzhel'sky, A. I. & Gulov, V. Y. Deformation of emulsion droplets in flow. *Colloid Polym. Sci.* **252,** 124–132 (1974).

71. Yang, Y. *et al.* Entropic Ligands for Nanocrystals: From Unexpected Solution Properties to Outstanding Processability. *Nano Lett.* **16,** 2133–2138 (2016).

72. Bigioni, T. P. *et al.* Kinetically driven self assembly of highly ordered nanoparticle monolayers. *Nat. Mater.* **5,** 265–270 (2006).

73. Kalsin, A. M. *et al.* Electrostatic self-assembly of binary nanoparticle crystals with a diamond-like lattice. *Science (80-.).* **312,** 420–424 (2006).

74. Edwards, E. W., Wang, D. & Möhwald, H. Hierarchical organization of colloidal particles: From colloidal crystallization to supraparticle chemistry. *Macromol. Chem. Phys.* **208,** 439–445 (2007).

75. Guo, J., Yang, W. & Wang, C. Magnetic colloidal supraparticles: Design, fabrication and biomedical applications. *Adv. Mater.* **25,** 5196–5214 (2013).